A proposal to Brookhaven National Laboratory to Measure
# Large Rapidity Drell Yan Production at RHIC

E.C.Aschenauer, A. Bazilevsky, L.C. Bland, K. Drees, C. Folz, Y. Makdisi, A. Ogawa, P. Pile,
T.G. Throwe
*Brookhaven National Laboratory*

H.J. Crawford, J.M. Engelage, E.G. Judd
*University of. California, Berkeley/Space Sciences Laboratory*

C.W. Perkins
*University of. California, Berkeley/Space Sciences Laboratory /Stony Brook University*

A. Derevshchikov, N. Minaev, D. Morozov, L.V. Nogach
*Institute for High Energy Physics, Protvino*

G. Igo
*University of California, Los Angeles*

M. Grosse Perdekamp
*University of Illinois*

M.X. Liu
*Los Alamos National Laboratory*

H. Avakian
*Thomas Jefferson National Accelerator Facility*

E.J.Brash
*Christopher Newport University and TJNAF*

C.F.Perdrisat
*College of William and Mary*

V. Punjabi
*Norfolk State University*

Li, Xuan
*Shandong University, China*

Mirko Planinic, Goran Simatovic
*University of Zagreb, Croatia*

A.Vossen
*Indiana University*

G. Schnell
*University of the Basque Country and IKERBASQUE, Spain*

A. Shahinyan, S. Abrahamyan
*Yerevan Physics Institute, Armenia*

16 May 2011

# I. Introduction

The Drell-Yan (DY) process is the annihilation of a quark from one hadron with an antiquark from a different hadron to create a virtual photon ($\gamma^*$) in the collision between two hadrons at center-of-mass energy $\sqrt{s}$. The hadrons are usually nucleons, and DY production is of interest both for collisions between free nucleons and when nucleons are bound in an atomic nucleus. The virtual photon from the DY process is experimentally observed by its decay into oppositely charged leptons, $e^+e^-$ or $\mu^+\mu^-$, called dileptons. Theoretical understanding of DY production in p+p collisions is thought to be robust [1].

Our experiment, called $A_N$DY, focuses on measuring di-electrons from the DY process at large rapidity, when the $\gamma^*$ has large longitudinal momentum, $p_z$. It is frequently more convenient to use the Feynman scaling variable, $x_F=2p_z/\sqrt{s}$, since in the parton model using a collinear factorized approach the virtual photon kinematics are related to the momentum fractions of the quark ($x_1$) and antiquark ($x_2$) via $x_F=x_1-x_2$ and $M^2=x_1x_2s$, where $M$ is the virtual photon mass. It is particularly interesting to consider large-$x_F$ DY production of low mass dileptons (M>4 GeV) from colliding transversely polarized proton beams, since this tests theoretical understanding of transverse spin effects. The collisions of protons (or deuterons) with heavy nuclei at RHIC at the largest $\sqrt{s_{NN}}$ possible at the facility provides access to low Bjorken-$x$ values in the nucleus. Large-$x_F$ dileptons produced from such collisions are very energetic, and such $e^+e^-$ dileptons are best detected using electromagnetic calorimeters aided by other detectors used to suppress prolific backgrounds. We propose to measure large-$x_F$ DY production for transversely polarized p+p collisions at $\sqrt{s}$=500 GeV and to establish the basic requirements for future upgrades of the RHIC facility that are aimed at a low-$x_2$ program.

We also propose to investigate DY di-electron production both inclusive and in coincidence with large rapidity $\pi^0$s from dAu beams at $\sqrt{s}$=200 GeV to determine the experimental requirements for measuring the parton distributions in nuclei. The apparatus is suitable for investigating $\Lambda$ and exotic particle production from AuAu interactions at $\sqrt{s}$=200 GeV, and we propose to take data with AuAu beams in exploring the far-forward region at RHIC and as required to calibrate the ZDCs.

This proposal covers Runs 12 and 13 at RHIC. Our primary goals for the project are:

I. to establish that large-$x_F$ low-M dileptons from the DY process can be discriminated from background in $\sqrt{s}$=500 GeV $p^\uparrow$+p collisions;

II. to provide sufficient statistical precision for the analyzing power for DY production to test the theoretical prediction of a sign change compared to transverse single spin asymmetries for semi-inclusive deep inelastic scattering.

Our goals for our tests in Run11 have been met:

11-1. we have established the impact of a third IR on RHIC performance for p+p collisions at $\sqrt{s}$=500 GeV, concluding that we can integrate >150 pb$^{-1}$ in 3IR operation without significant impact on STAR or Phenix

11-2. we have demonstrated a means of calibrating existing hadron calorimeter modules (Hcal) in the colliding beam experiment

Our specific goal for Run12 is:

12-1. to observe J/$\psi \rightarrow e^+e^-$, $\Upsilon \rightarrow e^+e^-$ and the dilepton continuum between these two signals as a clear benchmark for DY feasibility

Our specific goal for Run13 is:

13-1. to acquire a second data sample with integrated luminosity ~150 pb$^{-1}$ with tracking through the PHOBOS split-dipole field to quantify the role of charge sign discrimination in suppressing backgrounds

As discussed in section II, transverse single-spin asymmetries have been observed for large $x_F$ pion production in p$^\uparrow$+p collisions over a broad range of $\sqrt{s}$, extending to RHIC collision energies [2,3]. In the collinear parton model at leading twist, these spin effects are expected to be small. Transverse single spin asymmetry (SSA) effects are also observed in semi-inclusive deep inelastic scattering (SIDIS) from transversely polarized proton targets [4]. The large effects seen by experiments have resulted in extensions to the collinear parton model by the introduction of spin-correlated transverse momentum ($k_T$) to parton distribution and fragmentation functions. Spin-correlated $k_T$ has been observed for fragmentation functions [5], and probe transversity (transversely polarized quarks in a transversely polarized proton) through the Collins effect [6]. The Sivers effect [7] attributes the transverse spin effects to a correlation between the parton $k_T$ and the proton spin, corresponding to orbital motion of the partons within the proton. To be non-zero, the Sivers effect requires a final-state interaction in SIDIS that naturally arises to ensure gauge invariance [8]. Theoretical understanding predicts that the attractive final-state interaction in SIDIS becomes a repulsive initial-state interaction in DY thereby resulting in a sign change for the Sivers function between the two processes [9]:

$$f^{Sivers}(x,k_T)\Big|_{DY} = - f^{Sivers}(x,k_T)\Big|_{SIDIS}.$$

The objective of this experiment is 1) to acquire large enough data samples to establish that large-$x_F$ and low-$M$ dileptons from DY production can be discriminated from background in $\sqrt{s}$=500 GeV p$^\uparrow$+p collisions, and, 2) to provide statistical precision for the analyzing power for DY production to test the theoretical prediction. We recognize the importance of measuring the asymmetries for different products in the same $x_F$ and $k_T$ regions [10] and have instrumented A$_N$DY to measure DY electrons, $\pi^0$, and jets in similar kinematic regions. Our proposal will result in a measurement of DY that overlaps the kinematics of SIDIS, as required to test the predicted sign change.

Given that the primary objective is to intercompare a sign for a transverse SSA from two different processes, this point deserves some elaboration. Recent work [10] has recognized that the sign change predicted for DY production in relation to SIDIS is also expected for inclusive pion production, when there is a single dominant subprocess ($qg \rightarrow qg$) as is found by next-to-leading order pQCD calculations for pion production. The SIDIS measurements by the HERMES collaboration [11] span Bjorken $x$ values from ~0.02 to ~0.3. The pion production

3

measurements at RHIC energies typically show analyzing powers whose magnitudes increase with Feynman $x$ larger than 0.3. Positive and neutral pions are found to have a positive analyzing power and negative pions a negative analyzing power. The sign mismatch between the two processes has led to the suggestion that the Sivers function has a node at Bjorken $x{\sim}0.3$. To avoid any confusion regarding signs, $A_N$DY proposes to measure the analyzing power for DY production at $x_F$ values that will overlap those from SIDIS. As well, neutral pion analyzing power will be measured in the same range as for DY, and with some overlap with prior pion production measurements, limited to $x_F{<}0.4$ by the ability to robustly identify neutral pions.

Successful outcome of this experiment will establish requirements for future use of DY production to probe parton distributions to very low $x$. The lowest $x$ values are probed when dileptons are detected at large rapidity for p+p and p(d)+A collisions at the highest possible collision energies. To a very good approximation, the Bjorken-$x$ variable for the target antiquark is given by $x_2 \approx M^2/(x_F s)$. It can be imagined that RHIC could collide 250 GeV protons on 100 GeV/nucleon heavy ions in a future run, although technical difficulties associated with small velocity differences between the beams would need to be overcome for this to be realized. Detection of DY dileptons with $M{\sim}4$ GeV/c$^2$ at large $x_F$ can allow $x_2 \sim 10^{-4}$. Existing RHIC capabilities for d+Au collisions at $\sqrt{s_{NN}}{=}200$ GeV would probe down to $x_2 \sim 4{\times}10^{-4}$, albeit with some additional complexities given the spectator neutron. These momentum fractions and scales rival what can be achieved in eRHIC. The robustness of the theory leads to the expectation that *universal quantities* (unintegrated parton distribution functions) related to parton saturation would appear in p + A DY production and e + A deep inelastic scattering.

As detailed in section III, the basic requirements to discriminate $e^+e^-$ dileptons from background include electron/hadron discrimination (see Sec. IV) and electron/photon discrimination (see Sec. V). A major objective of this experiment is to establish if charge sign identification is a requirement to reduce backgrounds for our low-x future investigations (Sec. VI). Charge sign identification would require tracking through a magnetic field. For large rapidity dileptons, the natural means of identifying charge sign would be tracking through a dipole magnetic field, since deflections of large $x_F$ charged particles in a solenoid are small and the return yoke of a torroid blocks the relevant acceptance. Use of a dipole magnet in a colliding beam experiment is challenging, so establishing its requirement by a feasibility experiment is important. Space constraints at both STAR and PHENIX are severe and would involve major changes to integrate forward apparatus that meets the basic requirements for DY measurements at large $x_F$. Consequently, the experiment is best performed at a third interaction region (IR) as discussed in Sec. VIII. Timely completion of $A_N$DY is essential to enable designs for upgrading forward apparatus at STAR and PHENIX. Major forward upgrades are a focus of decadal plans for PHENIX and STAR.

As detailed in section IX, we see that RHIC operation for polarized proton collisions has involved different working points aimed at increasing dynamic aperture of the accelerator. These new working points have less severe effects from beam-beam tune shifts; a test with the new working point for $\sqrt{s}{=}500$ GeV polarized proton collisions in RHIC run 11 showed we can successfully integrate the required luminosity in 3 IR operation. In run-11 we took enough data to demonstrate a means of calibrating existing hadron calorimeter modules (Hcal, originally constructed for AGS E864) in the colliding beam experiment. As described in section VII,

spectra from the hadron calorimeter modules obtained in run 11, with energy scales set by $\rho^0 \rightarrow \pi\pi$, provide the first indication that our hadronic background estimates are robust.

In run 12, existing electromagnetic calorimetery (Jlab's BigCal) would be positioned at IP2 covering the hadron calorimetry. A timeline for the completion of the experiment is in section X. The experiment consists of two major runs. In RHIC run 12, the objective is to acquire as much as possible of the delivered ~170 pb$^{-1}$ integrated luminosity without a magnet. The estimated delivered luminosity uses the 56 pb$^{-1}$/week value at STAR and PHENIX from the May, 2010 RHIC projections for a 12 week polarized proton run at $\sqrt{s}$=500 GeV in run 12. The weekly delivered integrated luminosity is then scaled from the value for $\beta$*=0.5m to 14 pb$^{-1}$/ week for $\beta$*=2m that has been used at IP2 in prior runs. Power supplies for the IP2 focusing magnets (included in our cost estimates) could reduce $\beta$* further, and would be useful to improve the statistical precision of the transverse spin DY measurement. Observation of J/$\psi \rightarrow e^+e^-$, $\Upsilon \rightarrow$ $e^+e^-$ and the dilepton continuum between these two signals will be a clear benchmark for DY feasibility, given signal resolutions and the peak/background ratios.

In run 13, simple fiber tracking stations would be constructed and installed. In that run, the split-dipole magnet designed and operated by the PHOBOS collaboration at IP10 and moved to IP2 for this measurement, would be used to acquire a second data sample with large integrated luminosity. The May 2010 RHIC projections for a 12 week polarized proton run at $\sqrt{s}$=500 GeV in run 13 are 75 pb$^{-1}$/week at STAR and PHENIX. This would correspond to 18 pb$^{-1}$/week for $\beta$*=2m at IP2, meaning the total delivered integrated luminosity is estimated to be 225 pb$^{-1}$. The comparison of the two data samples will quantify the role of charge sign discrimination in suppressing backgrounds.

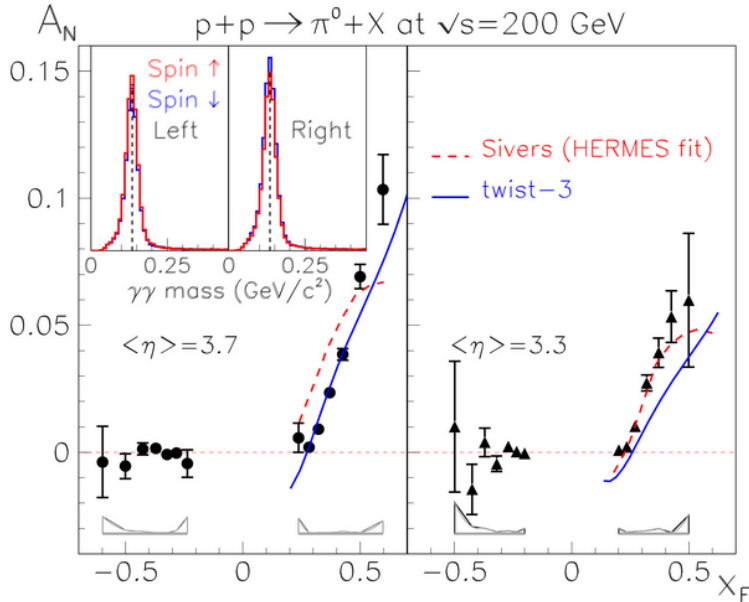## II. Physics addressed by large rapidity DY production



**Fig. II-1** Analyzing powers in $x_F$ bins at two different <$\eta$>. The Sivers calculation is based on a model [11] that fits semi-inclusive deep inelastic scattering data [12], as described in the text. The twist-3 calculation has subsequently been found to involve matrix elements related to moments of the Sivers function [13]. The inset shows examples of spin-sorted invariant mass distributions. The vertical lines mark the $\pi^0$ mass.

RHIC remains unique in the world given its capability to accelerate and collide spin polarized beams at center of mass energies where perturbative QCD has been demonstrated to provide a quantitative understanding of particle production over a broad range of transverse momentum and rapidity. The primary objectives of the RHIC spin program are to determine how the proton gets its spin from its quark, antiquark and gluon constituents. A major focus of the program, to date, has been the measurement of the contribution that possible polarization of the gluon field ($\Delta G$) makes to the spin of the proton. The observable at RHIC sensitive to $\Delta G$ is $A_{LL}$, corresponding to the ratio of helicity-dependent cross section difference to cross section sum for particle production. Measurements of $A_{LL}$ for neutral pion production, primarily from PHENIX [14], and jet production, primarily from STAR [15], are small and a recent global analysis [16] of world data has concluded that $\Delta G$ is small. In parallel with the completion of these $A_{LL}$ measurements, transverse single spin asymmetries (SSA) for particle production have been measured at RHIC and are found to be large, particularly for meson production in the forward direction [2,3]. The measured quantity is the analyzing power, $A_N$, corresponding to a left-right asymmetry of the produced particles when vertical polarization is used. A brief summary of findings for transverse SSA at RHIC

- Transverse SSA are observed at rapidites of produced pions $y_{beam}$-$y_\pi \leq 2$ [2,3], as shown in Fig. II-1, but are found to be zero at midrapidity [17].
- Non-zero SSA are observed at transverse momenta for the produced pions where pQCD is found to account for unpolarized cross sections ($p_T$>2 GeV/c) [18], as shown in Fig. II-2.
- Particle correlations show expected jet-like patterns [19], as shown in Fig. II-3.

These results have presented a challenge to theory. Sizeable $A_N$ are not expected in collinear pQCD at leading twist due to the chiral properties of the theory [20]. At $\sqrt{s}$=200 GeV, inclusive
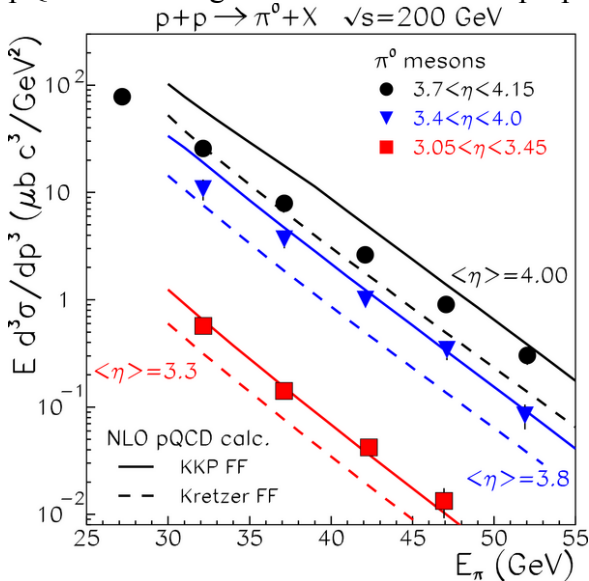


**Fig. II-2** Inclusive $\pi^0$ cross section for p+p collisions versus the leading $\pi^0$ energy ($E_\pi$) averaged over 5 GeV bins at fixed pseudorapidity ($\eta$). The error bars combine statistical and point-to-point systematic errors. The curves are NLO pQCD calculations using two sets of fragmentation
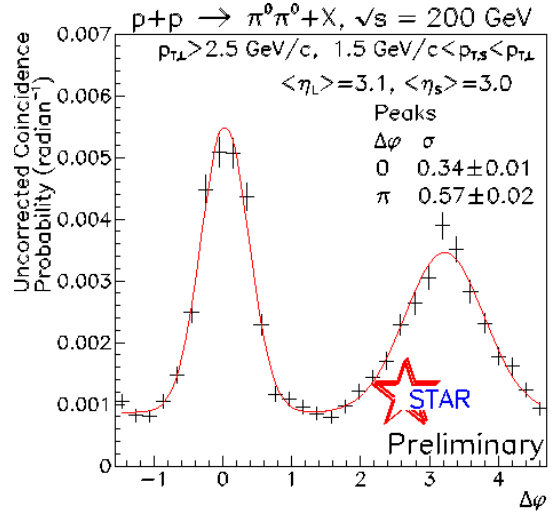
**Fig. II-3** Azimuthal correlation of forward di-pions show near- and away-side correlations in p+p as expected from di-jet production and have been demonstrated to be sensitive to the low-$x$ gluon density [19]. The data are fit by pairs of Gaussians and a constant background.

functions (FF).

pion cross sections at central and forward rapidity (Fig. II-2) are found to be in agreement with pQCD calculations above $p_T \sim 2$ GeV/c, and are included with world data for $\pi$ production from $e^+e^-$ collisions, semi-inclusive deep inelastic scattering and other p+p collider results in a global analysis of fragmentation functions [21].

Large $A_N$ are observed for inclusive pion production in $p^{\uparrow}$+p collisions over a broad range of collision energies [22]. For $\sqrt{s} \leq 20$ GeV, the cross sections are at least ten times larger than pQCD calculations for $x_F$ values where $A_N$ is sizeable [23]. This led to the suggestion that beam fragmentation, the dissociation of the polarized proton by the unpolarized target, was responsible for the spin effects, and the expectation that at sufficiently large $p_T$ these spin effects would vanish. Results from RHIC do not indicate this to be the case (Fig. II-4), with non-zero $A_N$ for pion production persisting to $p_T \sim 3.5$ GeV/c. There is no indication of a decrease of $A_N$ with increasing $p_T$. Similar $p_T$ dependence for other transverse SSA, such as induced polarization of hyperons produced in unpolarized hadroproduction reactions [24], has been observed but has to date eluded a robust theoretical understanding.

The observations of these large analyzing powers for pion production have prompted extensions to pQCD that introduce transverse momentum dependence (TMD) correlated with the spin degree of freedom. For example, $A_N$ could be generated by spin-correlated TMD fragmentation if there is transverse quark polarization in a transversely polarized proton ("Collins effect") [6]. Spin correlated TMD distribution functions ("Sivers functions") can explain a large $A_N$ [7]. These functions describe partonic orbital motion within the proton, and so are important for understanding the structure of the proton.
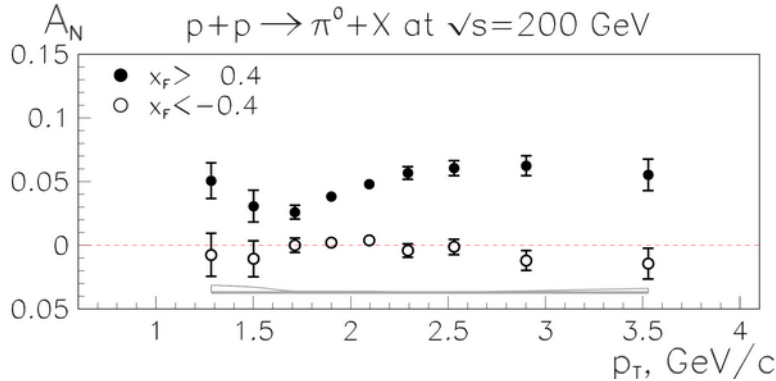


Fig. II-4 Analyzing powers versus $\pi^0$ transverse momentum ($p_T$) for events with scaled $\pi^0$ longitudinal momentum $|x_F| > 0.4$. Statistical errors are indicated for each point. Systematic errors are given by the shaded band, excluding normalization uncertainty.

Essentially concurrent with experiments at RHIC, first results for transverse SSA were obtained in semi-inclusive deep inelastic scattering [4]. In SIDIS, the mesonic fragments from the current quark in lepton deep-inelastic interactions are observed to vary with azimuthal angle for measurements with a transversely polarized proton target. The "Collins effect" can be separated from the "Sivers effect" in these measurements, and both are found to be non-zero. The "Sivers effect" requires a correlation of the form $\vec{S}_p \bullet (\vec{p}_{\pi} \times \vec{q})$, where $\vec{S}_p$ refers to the proton spin, $\vec{p}_{\pi}$ refers to the final-state pion momentum and $\vec{q}$ refers to the quark momentum. This triple product violates naïve time reversal, and so was initially thought to mean the "Sivers effect"

would vanish [6]. A color-charge interaction between the current quark and the spectators is required by gauge invariance, and results in the "Sivers effect" being an allowed leading-twist effect [8]. This color-charge interaction occurs in the final state in SIDIS, and is necessarily attractive [26], as expected since the proton is initially color neutral meaning that the current quark and the spectators must have equal magnitude but opposite sign color charges.

Phenomenological analyses of the "Sivers effect" from SIDIS have been made [12]. Model calculations [11] that presume that TMD distribution functions can be included in a factorized calculation are consistent with transverse SSA measured for pion production at RHIC energies, using the phenomenological fits to SIDIS results. As described below, there is no proof of factorization using TMD distribution or fragmentation functions for the hadroproduction of hadrons. A collinear approach using higher-twist quark-gluon correlators has been proven to have a factorized form for inclusive meson production [27]. Phenomenological fits to the quark-gluon correlators do give good descriptions of the $x_F$ dependence of inclusive meson production. Moments of the Sivers functions have been found to be related to the quark-gluon correlators in this approach [28].

It was quickly recognized by the theory community that the attractive final-state interaction in SIDIS becomes a repulsive initial-state interaction in the Drell-Yan production of a virtual photon. Present theoretical understanding of transverse SSA then predict that the sign of the analyzing power for DY will be opposite to that observed in SIDIS. **The test of this theoretical prediction is a primary objective for this experiment.**

Intense interest in the understanding of transverse SSA has resulted in numerous theoretical predictions of quantities sensitive to the color-charge interactions. An example was the prediction that di-jet momentum imbalance would be correlated with spin [29], and would serve to test the "Sivers effect" observed in SIDIS. A measurement was completed [30], and the result was compatible with zero spin dependence. Subsequent theoretical work established that the color structure of the diagrams contributing to di-jet production is complex, and leads to cancellations between "SIDIS-like" attractive final-state interactions and "DY-like" repulsive initial-state interactions. The end result is that these results have stimulated theorists to recognize the complexities of color charge interactions, with the conclusion that there is no factorization for TMD distribution or fragmentation functions in p+p interactions that produce hadronic final states. This is in contrast to the case for DY production, where robust factorization theorems exist and are thought to be still valid, since the color structure of the process is particularly simple.

There are plans by many other laboratories to measure transverse SSA in DY production. Only one other plan has time scale comparable to that of this proposal. The COMPASS collaboration plans to measure the analyzing power for DY production using high-energy pion beams incident on a transversely polarized proton target. They will propose measurements of generalized parton distributions with a polarized muon beam, followed by measurements of pion induced DY production from a transversely polarized proton target, with the hope of embarking on these measurements in 2013.

At RHIC, PHENIX is ready to make a measurement of transverse SSA for DY production by observing dimuons in their muon arms. Their J/$\psi$ measurements at $\sqrt{s} = 200$ GeV have been published [31]. The rapidity coverage of the muon arms results in most of this data having $x_F < 0.1$ (see Fig.II-1).

The most recent update (2008) to Performance Measures by the Nuclear Science Advisory Committee [32] added the milestone *test unique QCD predictions for relations between single-transverse spin phenomena in p+p scattering and those observed in deep-inelastic lepton scattering*, with an estimated completion of 2015. The HP13 milestone is recognition by the nuclear physics community of the scientific importance of transverse SSA measurements that would robustly test present-day theoretical understanding. Completion of the DY feasibility experiment proposed in this letter of intent on the timescale described in section X would then complete the HP13 milestone, and should get first results for a transverse SSA measurement for DY production.

It is useful to have perspective on what would be learned when this transverse spin DY experiment gets completed. An experiment that finds $A_N$ for DY production to be zero, with a precision of $\delta A_N \sim 0.01$, would mean that present understanding is not a complete way of describing transverse SSA measured for semi-inclusive deep inelastic scattering and that measured for pion production analyzing powers. A non-zero $A_N$ for DY production would be consistent with the presence of a correlation between the spin of the proton and the intrinsic transverse momentum of its constituent quarks. **Such a correlation requires orbital motion of quarks within the proton**. The ability to relate this to the understanding of the spin of the proton is still being debated in the community. A non-zero and negative $A_N$ for DY production, as predicted by theories that include the gauge link, would suggest that the $k_T$ factorization for DY production is indeed robust. An intuitive way to view the gauge link impacts on DY and on semi-inclusive deep inelastic scattering is that unlike colored charges have an attractive interaction and like colored charges have a repulsive interaction. A non-zero and positive $A_N$ for DY production, opposite to theories that include the gauge link, would challenge $k_T$ factorization theorems for the DY process. These theorems are the way to understand how an infrared divergence associated with the transverse momentum of the virtual photon going to zero leads to zero yield. That technical statement has an intuitive interpretation that the colored charges within the proton are distributed in such a way that a picture of a point-like color charge producing a field through which a quark propagates before annihilating with an antiquark to produce a virtual photon is too simplistic.

## III.  Basic requirements for large rapidity DY production

The original Drell-Yan planning document [33] submitted for consideration to the 2007 Long Range Plan by the Nuclear Science Advisory Committee had concluded that a transverse spin DY measurement at RHIC would be best done at $\sqrt{s}$=200 GeV, although this depended on the rapidity coverage of the apparatus. A primary component of this conclusion was to allow concurrent measurements by STAR and by PHENIX. As discussed below, the experiment we propose is best conducted for p+p collisions at $\sqrt{s}$=500 GeV.

It is useful to reiterate some of the discussion from reference [33]. The hard-scattering, partonic-level cross section ($\hat{\sigma}$) for $q\bar{q} \rightarrow \gamma^*$ is proportional to $1/\hat{s}$, where $\hat{s}$ is the squared collision energy in the partonic center of mass. The DY cross section for p+p→γ*+X is a convolution of $\hat{\sigma}$ with quark and antiquark distribution functions. Frequently, analyses of particle production rates discuss partonic level luminosities, accounting for the distribution functions. In this view, it is simply the increased partonic level luminosity resulting from increased low-x parton densities that results in larger di-lepton yields as the collision energy is increased.
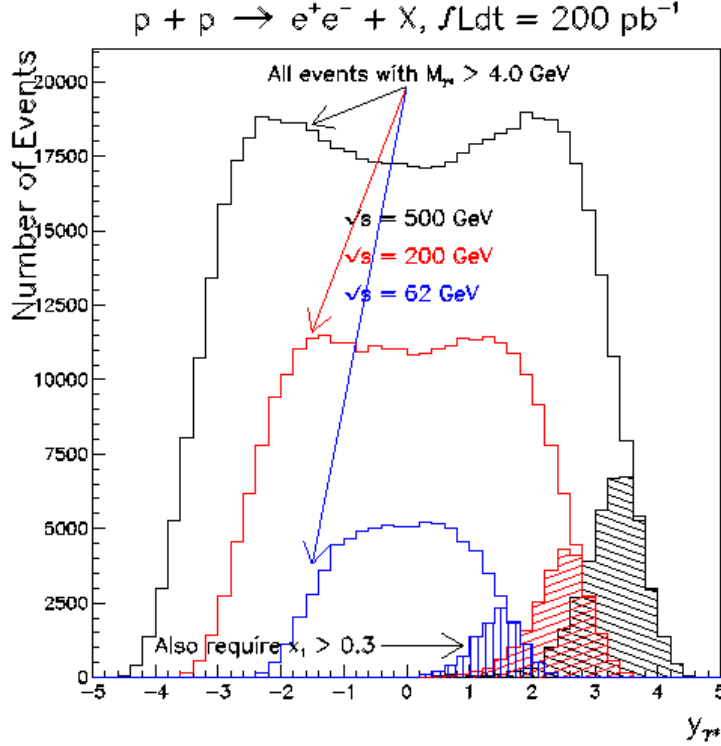


**Fig. III-1** The number of di-electron events from virtual photon production with mass greater than 4 GeV/c$^2$ as simulated by PYTHIA 6.222, distributed according to the rapidity of the virtual photon. The integrated luminosity is assumed to be fixed at 200 pb$^{-1}$ for all collision energies considered. As the collision energy increases, the rapidity distribution broadens, given the increased phase space. As the collision energy increases, the di-electron cross section increases, even though the hard scattering DY cross section decreases. The increase in the di-electron cross section is a consequence of an increase in the partonic luminosity as the collision energy increases.

Another reason that polarized proton collisions at the highest RHIC energies minimize the running time for a transverse spin DY experiment is the growth of the collision luminosity with √s, caused by the smaller transverse size of the beams at higher energy.

A result of all of these considerations is that √s=500 GeV polarized proton collisions provide the ideal collision energy for a DY experiment.

A result from RHIC run 8 with STAR's Forward Meson Spectrometer (FMS) [34] has implications for our transverse SSA measurement for DY production at large rapidity. Such a measurement focuses on dilepton masses that lie between the J/ψ and the ϒ, so as to obtain sufficient statistics. Large-$x_F$ J/ψ production in p+p collisions was observed by the FMS through the J/ψ→e$^+$e$^-$ decay channel (Fig. III-2).

The run-8 data were analyzed to look for large-mass cluster pairs. A peak is observed with significance 4.5σ at the mass consistent with expectations for J/ψ→e$^+$e$^-$. The event

reconstruction utilizes a bare electromagnetic calorimeter response, given that no tracking data was available.
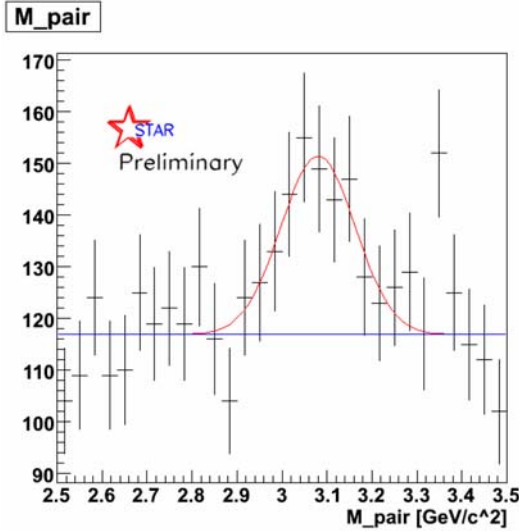


**Fig. III-2** Reconstructed mass from pairs of clusters observed at forward rapidity with the Forward Meson Spectrometer (FMS) at STAR. Each cluster is subjected to an isolation cut, to reduce backgrounds from neutral pion decay and jet production. A further requirement is imposed on the transverse momentum of the cluster. The Gaussian peak is consistent with observation of J/$\psi$ produced with $<x_F>=0.67$. The $x_F$ dependence of J/$\psi$ production in p+p collisions could come from large-x intrinsic heavy components in the proton wavefunction [35].

Ongoing work has established that the large-mass background is well described by PYTHIA 6.222 + GEANT simulation. That simulation identifies the background as primarily photons, coming from neutral pions that are fragments of partons that get scattered to large rapidity from highly asymmetric initial states (primarily large-$x$ quarks incident on low-$x$ gluons). The hadronic content of the background is small, given that the EMCAL has only ~1 hadronic interaction length, meaning that its high-energy (E>30 GeV) response is dominated by incident photons, electrons and positrons. This background can be reduced by identifying whether the particle incident on the calorimeter is charged or neutral. Photon conversions that primarily occur from exiting the beam pipe limit the utility of background reduction via neutral/charged tagging, although the conversions do result in a different transverse profile of the calorimeter response that can aid the suppression of this background. So, the first two requirements for the experiment are (1) robust discrimination between neutral and charged showering particles; and (2) robust discrimination against the prolific charged hadrons as deposited energy in the EM calorimeter is lowered.
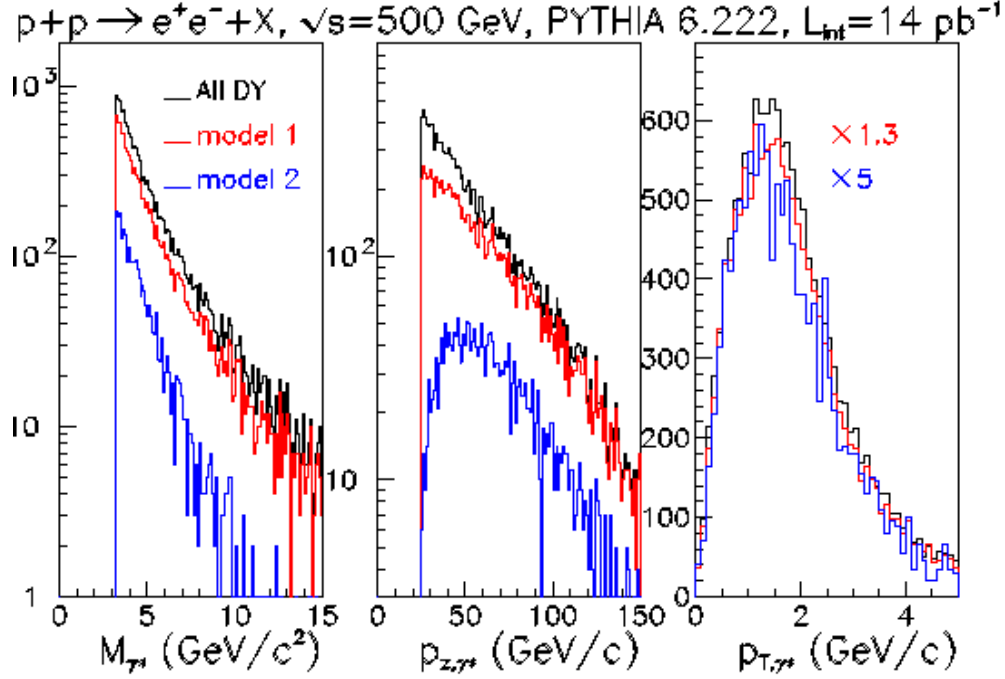
11

**Fig. III-3** Kinematic distributions for the virtual photon. Model 1 would be a final facility and model 2 is the first stage of the proposed feasibility test for studying DY production at RHIC.

Kinematic distributions showing the $M$, $p_z$ and $p_T$ dependence of virtual photons that decay to $e^+e^-$ dileptons for p+p collisions at $\sqrt{s}=500$ GeV are shown in Fig. III-3. These distributions are from PYTHIA 6.222. The virtual photon mass distribution is proportional to $M^{-3.3}$, which is a somewhat more rapid $M$ dependence than expected for no scaling violations. The $p_z$ distribution is consistent with the cross section varying like $(1-x_F)^5$, as expected from the structure functions. The momentum distribution and the $x,y$ intercepts at the electromagnetic calorimeter for the electrons and positrons from the virtual photon decay are shown in Fig. III-4. Model 1 in these figures refers to a final DY facility that would include a $(2m)^2$ electromagnetic and hadronic calorimeter with a central $(0.2m)^2$ hole for the beam pipe positioned 10m from the interaction point. Model 2 refers to our proposed setup consisting of two 9×12 arrays of existing hadron calorimeters originally built for AGS-E864 [36], with modular electromagnetic calorimeters 500 cm from the interaction point. Since the longitudinal momentum of the virtual photon is large, the polar angles associated with $\gamma^*$ will be small. Consequently, there will be large probability for the leptons from the $\gamma^*$ to be on opposite sides of the beam line. The azimuthal orientation of the virtual photon transverse momentum will be determined by the measurement of the daughter lepton momenta. Many, although not all, earlier dilepton experiments measured charge sign of each lepton, to enable background subtraction from the unlike-charge sample by the like-charge sample. It can be experimentally established in a staged approach to the DY feasibility test whether charge sign measurements are required. Charge sign measurements require magnetic analysis and tracking, as will be employed in run 13 in the third stage of this proposal.
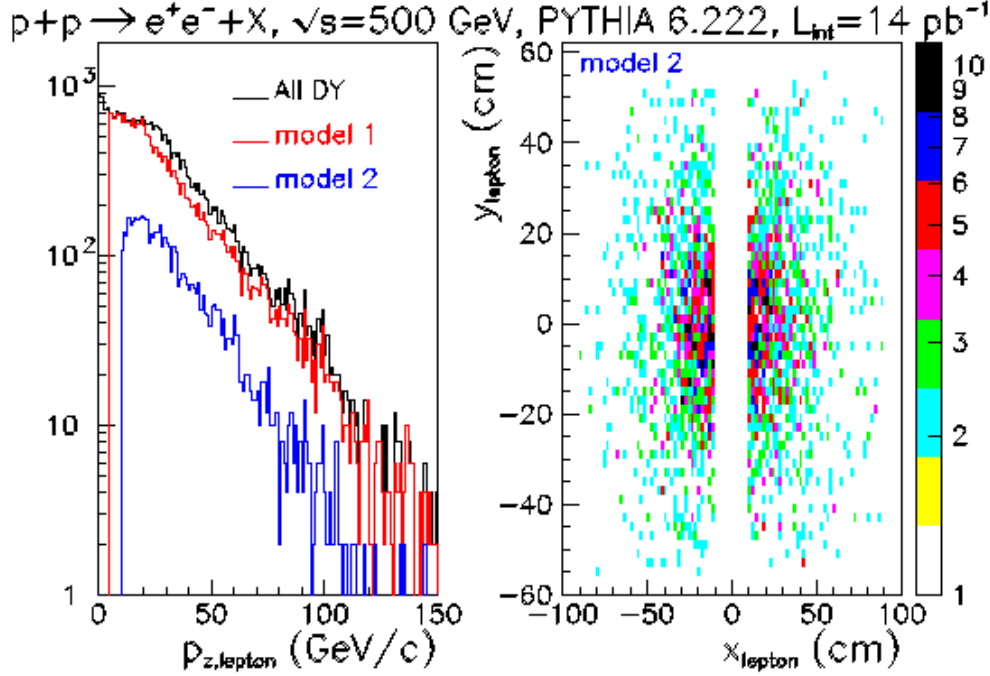
**Fig. III-4** Kinematic distributions for the electron and positron decay products of the virtual photon. Model 1 would be a final facility and model 2 is the first stage of the proposed fexperiment  for studying DY production at RHIC.


# IV. Electron/hadron discrimination

The Drell-Yan process in pp collisions at √s=500 GeV has a cross section of ~7x10$^{-5}$mb, which is a factor ~10$^6$ smaller than the 30mb of hadronic interaction cross section. One of the experimental challenges is to separate lepton signals from hadron backgrounds by roughly three orders of magnitudes per particle.

The electromagnetic calorimeter (EMcal) alone is a powerful tool to reduce hadron backgrounds. The response of 3.8 cm × 3.8 cm × 45 cm lead glass bars of the type from IHEP, Protvino, as used in BigCal and in our test of run11 to charged pions with E>15 GeV tracked to be within a 1-cell perimeter fiducial volume of an EMcal is simulated by GEANT.  The EMCal constitutes ~1 hadronic radiation length, hence ~50% of the charged hadrons leave very little energy (MIP) in the EMCal, while the remaining hadrons start to shower in the EMCal and deposit a fraction of their energy. The summed energy deposition in the EMcal ($\Delta E$) for each event is computed.  The ratio $f=\Delta E/E_{hadron}$ is formed.  The resulting probability distribution dN/d$f$ is established by scaling the frequency of observing $f$ by the number of incident hadrons.  The dN/d$f$ distribution above the MIP peak is quantitatively represented by a linear function of $f$, as shown in Fig. IV-1.
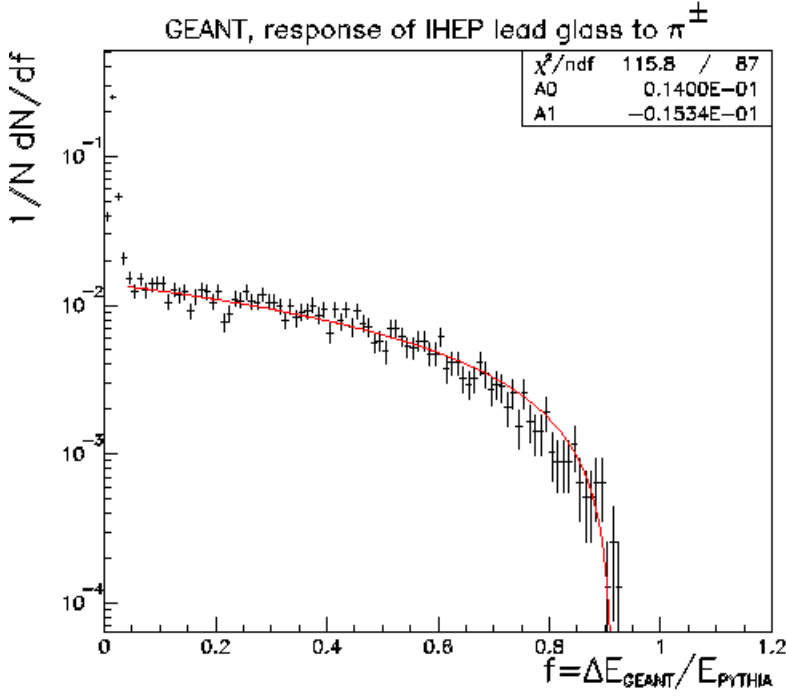
**Fig. IV-1** GEANT simulation of energy deposited in an EMcal built from 3.8 cm × 3.8 cm × 45 cm lead glass bars. Charged pions with E>15 GeV are used in this simulation. The fraction of the incident pion energy deposited in the EMcal is $f$. The dN/d$f$ distribution is well represented by a linear function of $f$, at values larger than the peak from minimum-ionizing particles.

This linear parametrization of the EMCal response to hadrons is used in a fast simulation method to estimate signal and background rates as described in the section VII. However it is important to note that there is significant model dependence in the EMCal response to hadrons as shown in Fig.IV-2.
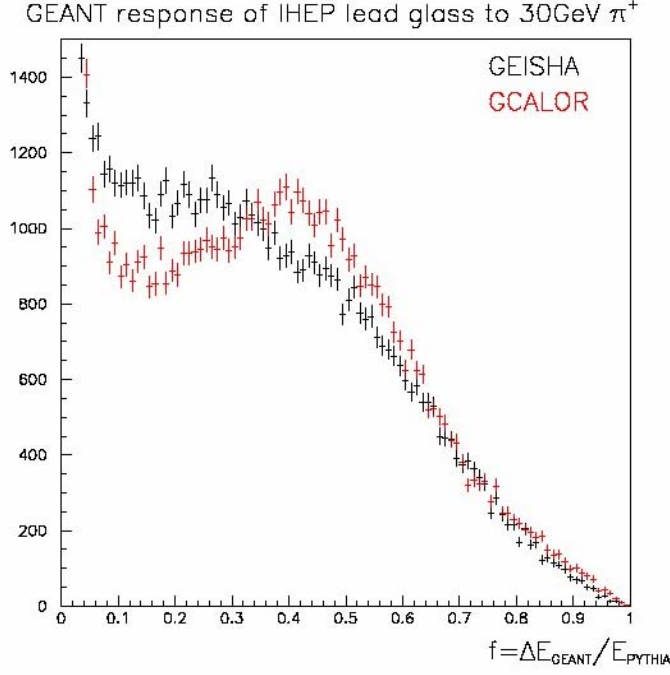
**Fig. IV-2** GEANT simulation with hadronic interaction package GEISHA (black) and GCALOR(red) of energy deposited in an EMcal built from 3.8 cm × 3.8 cm × 45 cm lead glass bars. Charged pions with E=30 GeV are used in this simulation. The fraction of the incident pion energy deposited in the EMcal is *f*.

The hadronic calorimeter (Hcal), modeled after the AGS-864 hadron calorimeter [36], consist of two 9x12 arrays of lead - scintillating fiber towers with resolution $\delta E/\sqrt{(E)} = 0.344/\sqrt{(E)}$. Geant was used to simulate responses of EMcal and HCal to 30GeV electrons and charged pions. A 3x3 cluster was formed around the high tower in the EMCal. The particle trajectory from the vertex to the EMCal high tower is projected onto HCal, and the 3x3 cluster energy deposit sum is computed. Distributions of the ratio R=ΔE(EMcal)/ (ΔE(EMcal)+ΔE(Hcal)) for electons and charged pions are shown at the top of Fig.IV-3. A simple cut on the ratio R>0.9 is more than 99% efficient in detecting electrons while rejecting ~82% of the hadrons. Remaining hadrons have an observed energy fraction f whose average is ~0.5.

For that small fraction of hadrons which deposit a high fraction of their energy in EMcal, hadron rejection using EMcal and Hcal is inefficient. For hadrons with f>0.7, the cut on R>0.94 rejects 40% of hadrons as shown in Fig.IV-4. We note that the development of electromagnetic and hadronic showers in EMcal is quite different and transverse shower shape information can be used to differentiate between electrons (and photons) and hadrons. We are currently investigating this option to quantify the rejection factor using this method.
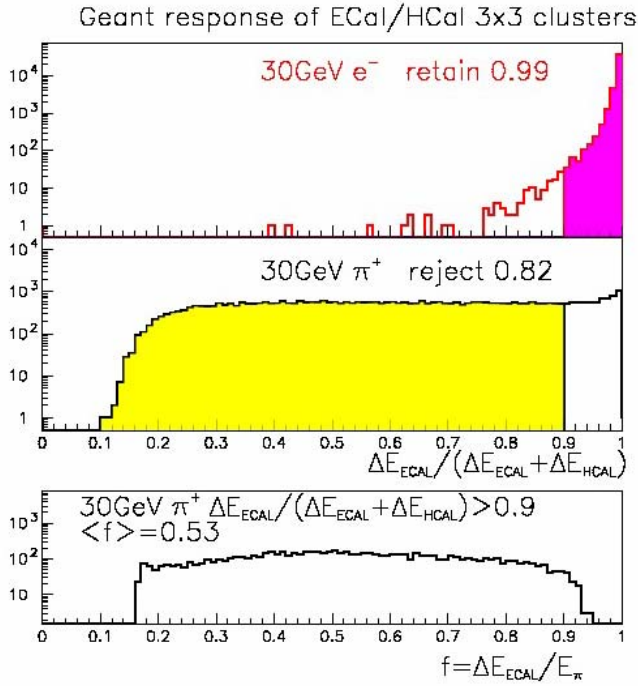
**Fig. IV-3** GEANT simulation for energy deposit in an EMcal and Hcal for 30GeV electrons and charged pions. A 3x3 cluster sum of deposited energy forms the ratio R=ΔE(EMcal)/(ΔE(EMcal)+ΔE(Hcal)) shown in top plot. With R>0.9 cut, EMcal+Hcal can reject 82% of hadrons while retaining 99% of electrons. The bottom plot shows distribution of f for hadrons who survives R>0.9 cut.
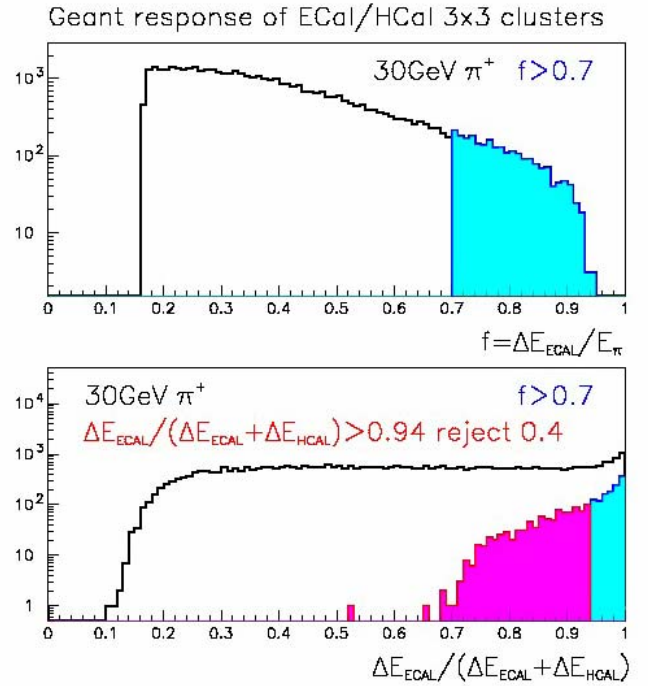
**Fig. IV-4** GEANT simulation for energy deposit in an EMcal and Hcal for 30GeV charged pions. The top plot shows the distribution of f in EMcal 3x3 clusters around the high tower. The bottom plot shows the ratio R=ΔE(EMcal)/(ΔE(EMcal)+ΔE(Hcal)). Blue shaded area is for hadrons surviving cut f>0.7. Red shaded area is hadrons which can be identified using Hcal by R>0.94 cut. This gives 40% hadron rejection for hadrons with f>0.7.

A detector in front of EMcal to measure early EM showers provides another way to reject hadrons. Responses of a pre-shower detector composed of 1cm Pb converter sandwiched between two 0.5cm scintillation plastic counters were simulated using Geant 3.21. Most of the electrons (and positrons) begin to shower in the lead converter plate with ~2 radiation lengths and can be identified as such in the second pre-shower scintillation counter. Meanwhile hadrons are unlikely to shower in the lead converter plate, since 1cm of lead constitutes only 5.7% of a hadronic interaction length. As shown in Fig.IV-5, use of such a pre-shower detector should allow identification of ~98% of electrons while rejecting ~86% of the hadrons.
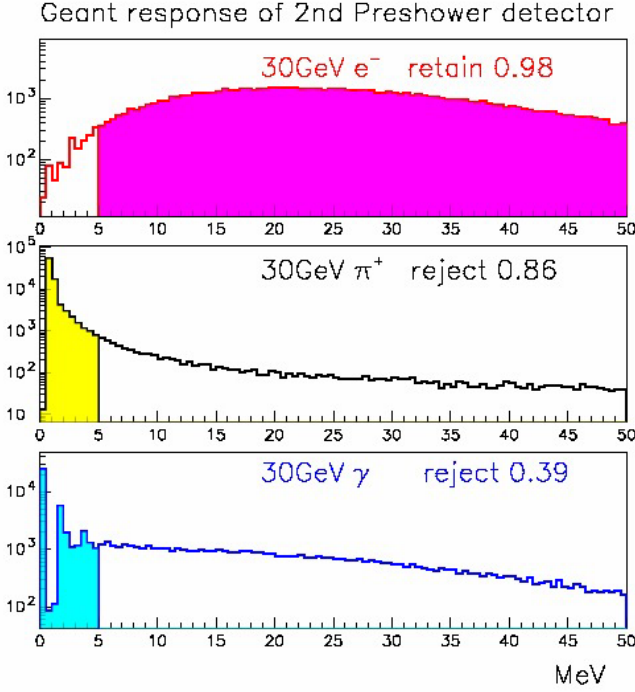
**Fig.IV-5** GEANT simulation of $2^{nd}$ pre-shower detector made of 0.5cm thick plastic scintillation counter placed after 1cm Pb converter. Responses for 30GeV electrons, charged pion and photons are simulated. A cut of energy deposit in the $2^{nd}$ pre-shower above 5MeV will retain 98% of electrons, while rejecting 85% of pions and 39% of photons.

Finally we intend to use the PHOBOS magnet as a spectrometer with tracking prior to the EMcal to discriminate electrons and positrons from charged hadrons using E/p, where E would be measured by the EMcal and p would be determined from the tracking (Sec. VI).

In section VII, hadron background rates were estimated using fast MC method, using parameters constrained by GEANT simulation described in this section.

## V. Photon/electron discrimination and conversion photon backgrounds

Photons are another major background, and they mostly come from meson decays. The pre-shower detector in front of EMCal is used to separate photons from electrons or positrons seen in EMCal. Some photons will be converted to electron positron pairs in upstream materials. The Be-beam pipe can be up to ~16% of a radiation length for the most forward angle we consider. At high energy (>~10GeV), the opening angle of the conversion $e^+e^-$ pairs is small, and the pre-shower detector can be used to identify them by separating 2MIP response from 1MIP. There is a small probability that photons convert in the pre-shower detector itself. Only ~½ of those can be distinguished from real electron/photon signals using the pre-shower detector.

An array of the 0.5cm thick plastic scintillator pre-shower counters is considered. Response of the detector to electrons and photons is simulated by GEANT and shown in fig.V-1. The simulation shows 98% of photons can be identified, while retaining 86% of the electrons or positrons.
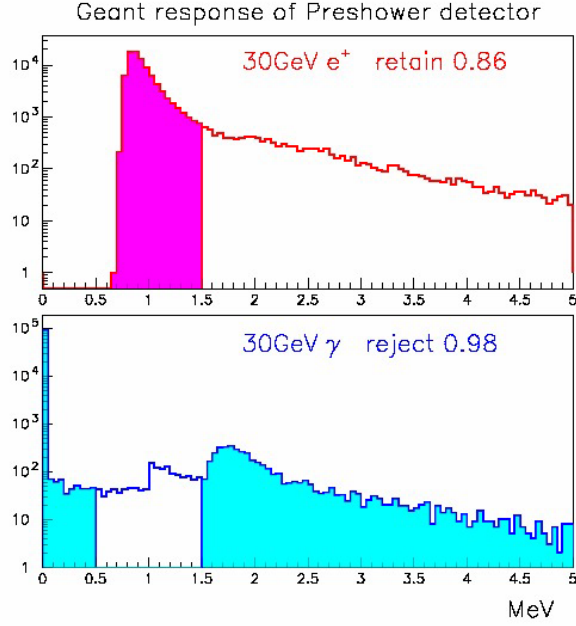
**Fig.V-1** GEANT simulation of a pre-shower detector made of 0.5cm thick plastic scintillation counter. Responses for 30GeV electrons and photons are simulated. A cut of 0.5MeV < dE < 1.5MeV will retain 86% of electrons, while rejecting 98% of the photons including ones converted to e+e- pairs in beam pipe and preshower detector itself.

The Second pre-shower detector after the ~2 radiation length of Pb converter was discussed in the previous section as a way to identify hadrons. Since photons start EM-showers slower than electrons or positions, GEANT simulation indicates moderate (~40%) photon rejection with the same cut used for hadron rejection, while retaining 98% of electrons or positrons, shown in Fig.V-1.

Over 90% of the photons are from the decay of neutral pions. By reconstructing neutral pions from the EMcal responses we can further suppress >90% of the remaining photons in the offline analysis. When charged particle tracking with a magnetic field is available, tracking can identify conversion $e^+e^-$ pairs to help further photon background rejection.

In section VII, photon background rates were estimated using fast MC methods, using parameters constrained by GEANT simulation as described in this section.

## VI. Charge sign discrimination

Charge sign for a particle produced in collisions between the two beams is determined by measuring the deflection of the particle through a magnetic field. The proposed implementation for this experiment is the split-dipole magnet designed, built and operated by the PHOBOS collaboration [37]. The magnet is presently at IP10, and must be removed for the future installation of electron lenses. The split-dipole magnet is designed to have minimal magnetic field along its symmetry axis, corresponding to the line along which the two beams move near the interaction point (IP). The dipole field is vertical, and has opposite-sign magnetic fields left and right of the beam line, with essentially zero field along the beam line. The coils are shaped in the *x-z* plane to meet the PHOBOS design criteria. For our purposes, the *x-z* shaping is moved further from the IP by a 180° rotation of the magnet about a vertical axis in comparison to the original magnet orientation at IP10 [37]. The magnet field map and geometry specification used

in the PHOBOS GEANT simulation were provided for our studies. A view of the magnetic field in the *x-z* plane at *y*=0 is shown in Fig. VI-1.
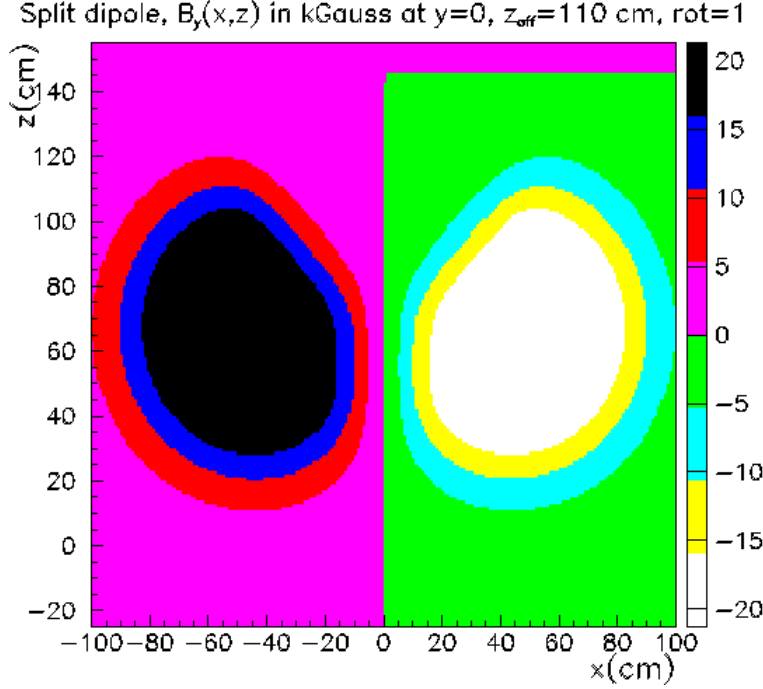


**Fig. VI-1** Map of the split-dipole magnet for the charge-sign discrimination stage of the $A_N DY$ experiment. The vertical component of the magnetic field is shown in the *x-z* plane at *y*=0. The interaction point is at *x=z*=0. Compared to the orientation used by the PHOBOS collaboration [37], the magnet is rotated by 180° around the *y* axis, so that the aperture restriction from the coils is at the smallest possible *z* value. This map is used for tracking charged particles produced by PYTHIA using routines from GEANT.

There are multiple challenges for charge-sign determination for DY production of virtual photons at large $x_F$. The electron and positron momenta are large as shown in Fig. III-3, meaning that bend angles in magnetic fields produced by conventional magnets are small. The electrons and positrons are produced at small polar angles, meaning that the distance along the beam line when they cross the 3.81 cm radius beryllium pipe is large. To minimize the extent of the z-crossing distribution, it is essential that the 9MHz RF system be operational. Estimates are [38] that the vertex distribution will be three times smaller than in all prior p+p runs. We assume a Gaussian distribution for the vertex-*z* distribution for the colliding beams characterized by $\sigma_z$=20 cm for the studies below. Tracking electrons and positrons produced by DY by PYTHIA 6.222 through the split-dipole field (Fig. VI-1) results in a distribution of *z* locations at the beam pipe, as shown in Fig. VI-2. The most recent RHIC projections expect $\sigma_z$=30 cm. Simulation differences between $\sigma_z$=30 cm and $\sigma_z$=20 cm are small.
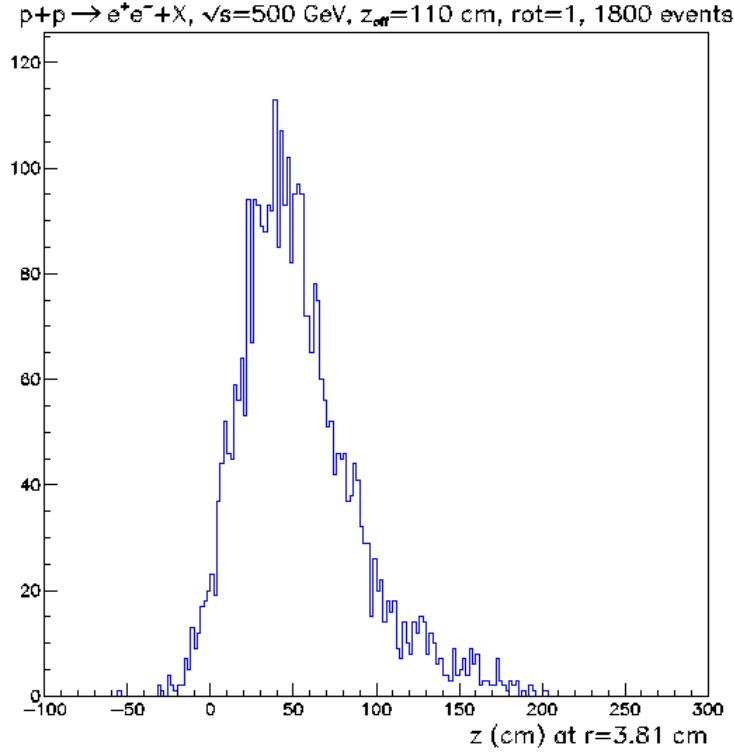
**Fig. VI-2** Distribution of *z* location of where electron and positron tracks cross the beam pipe. The collision diamond is modeled by a Gaussian distribution with $\sigma_z$=20 cm, as expected when the 9MHz RF system is used.

The minimal information to determine charge sign consists of three space points for each charged track. In a thin-lens approximation, the magnetic field produces a momentum impulse. The three points correspond to determining the line prior to the impulse and the point after the impulse, to establish the deflection. Given that colliding beam operation requires stable transverse position of the beams, a good measurement of the vertex z location for each event can establish one of the space points. The multiplicity of charged hadrons accompanying DY production can be used for that purpose. We propose three tracking stations for each module. The first two tracking stations are as close to the vertex as is practical, given the pipe-crossing distribution and the aperture constraints from the magnet, and are planned to be planes of scintillating fibers. The third tracking station is proposed as a large 2-plane fiber-scintillator array. The location of the tracking stations in relation to the electron and positron trajectories computed from tracking through the split-dipole field are shown in Fig. VI-3.
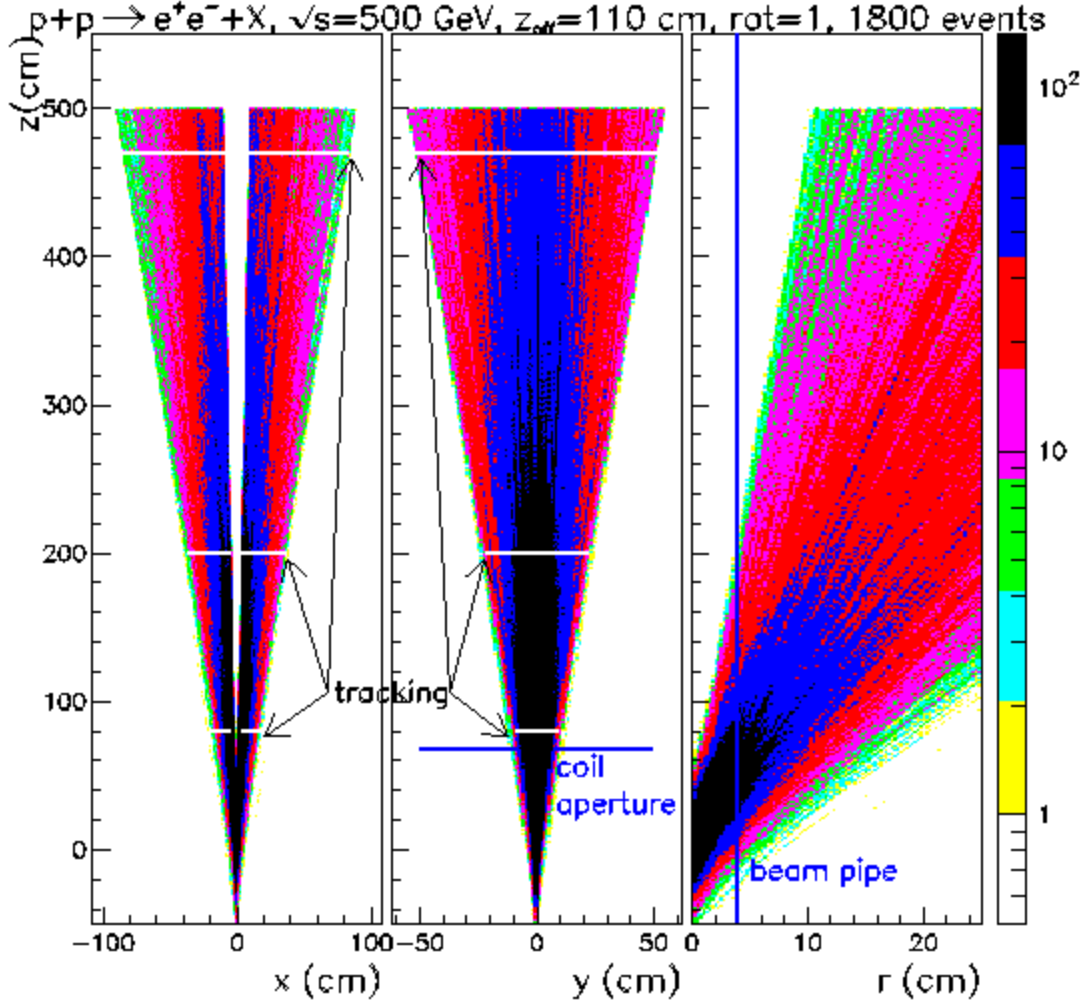
**Fig. VI-3** Overlay of electron and positron trajectories for 1800 DY events from tracking through the split-dipole field (Fig. VI-1). The left plot shows the trajectory in the *x-z* plane, the middle plot shows the trajectory in the *y-z* plane and the right plots shows the trajectory in the *r-z* plane. The location of the split-dipole magnet results in a vertical aperture limitation as shown. The *z* location of tracking stations is shown. The vertex z location can be measured from charged hadrons from the underlying event that intercept all three tracking stations.

The first two tracking stations at *z*=80 and 200 cm are proposed to be constructed from 2-mm square scintillating fiber ribbons. Each station would have *u-v* planes. The fiber size and number of fiber planes at each station are chosen to minimize the construction cost. The fibers are planned to run along the diagonal of the rectangle defining the active area of each tracking station. A minimum fiber length of 5 cm is assumed. Fig. VI-4 shows the x-y intercepts of the electron and positron trajectories at the *z*=80 and 200 cm fiber-tracking stations. The fiber count in the figure is for one u plane. The total channel count for the proposed implementation is 4× larger.
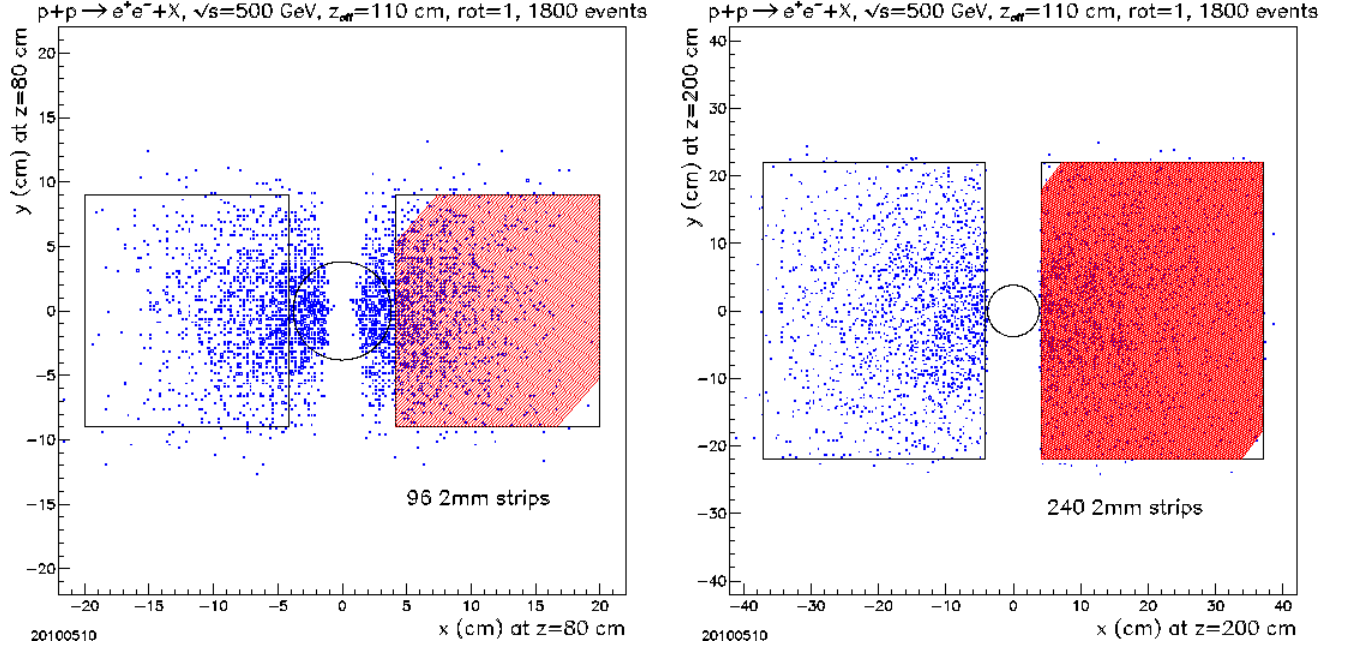
21

**Fig. VI-4** Electron and positron trajectory intercepts in the *x-y* plane at the *z*=80 cm tracking station (left) and the *z*=200 cm tracking station (right). The 3.81-cm radius beam pipe is indicated. Each plane is tiled by 2-mm square scintillating fibers of minimum length 5-cm chosen to be parallel to the diagonal of the rectangular area of the tracking station. In total each station would have four *u-v* scintillating fiber planes, of which only the *u*-plane is shown. Total scintillating fiber count is 1344 channels for the first two stations.

The fiber planes will consist of multi-fiber ribbons, clad by acrylic. The mechanical support for the ribbons will be from C-shaped clamps to hold the ribbons. A very thin vertical strut will complete the frame along the side of the fiber tracker closest to the beam pipe, so as to ensure that the active area can be as close to the pipe as possible. The framework will be held by supports attached to the magnet return yokes for the *z*=80 cm station. The framework for the *z*=200 cm station most likely will be supported by a stand attached to the floor. Material thicknesses for the tracking stations must be minimized to reduce photon conversions and bremsstrahlung of electrons and positrons when they traverse the detector. Bremsstrahlung in the air gaps could be minimized by the use of helium bags.

To demonstrate that the split-dipole and the proposed tracking stations will determine charge sign, the distance ($\Delta r$) in the *x-y* plane between a zero-field trajectory and the trajectory through the split-dipole magnet is computed for each electron and positron from DY production. The distribution of the $\Delta r$ at the *z*=80, 200 and 470 cm tracking stations for electrons and positrons from 1800 DY events is shown in Fig. VI-5.
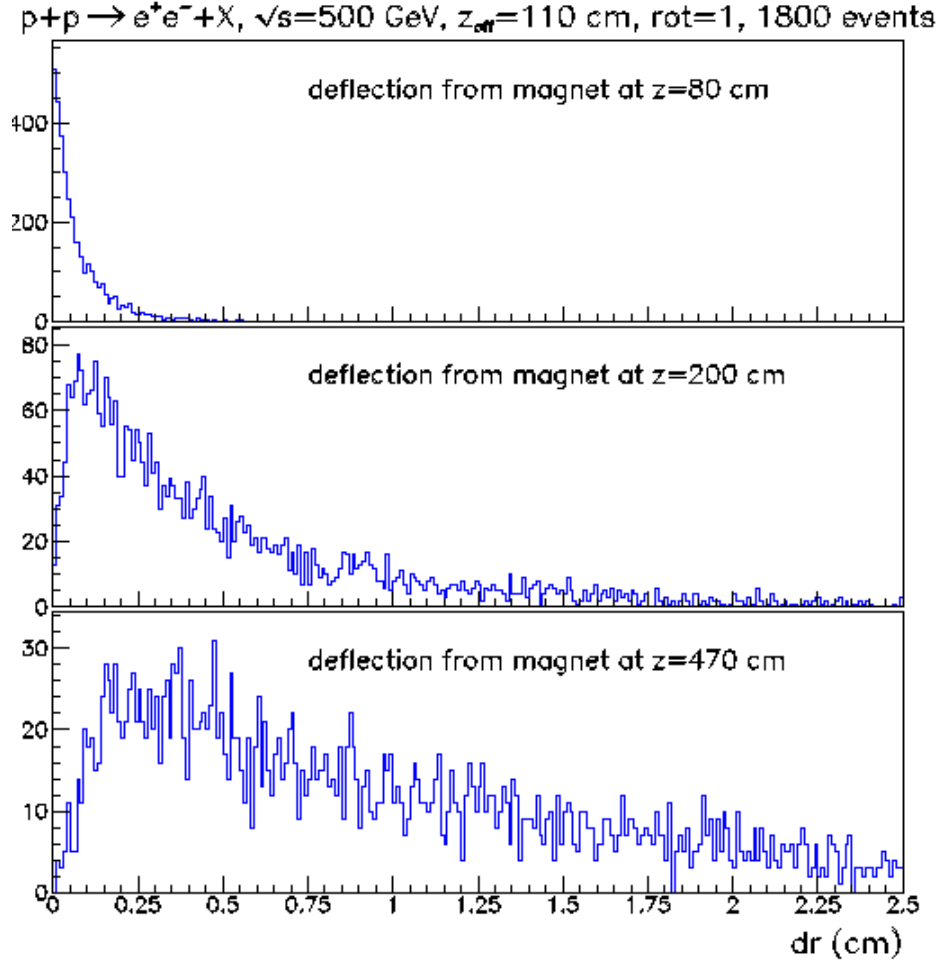
**Fig. VI-5** Distribution of distance in the *x-y* plane at each tracking station between a zero-field trajectory and full-field trajectory.

## VII.  Count rates and background estimates

Background estimates are made by using PYTHIA 6.222 to model p+p collisions at $\sqrt{s}$ = 500 GeV, and using fast simulation methods of detector response, constrained to full GEANT studies as described in earlier sections.  This strategy was followed because of order $10^{12}$ p+p interactions at $\sqrt{s}$=500 GeV must be considered to estimate background in comparison to DY production.  Extensive comparisons of PYTHIA 6.222 to particle production cross sections have been conducted for p+p collisions at $\sqrt{s}$ = 200 GeV [39].  In general, PYTHIA 6.222 accounts for the observed yields at large rapidity.  Later versions of PYTHIA now exist, and generally involve specific tunes aimed at understanding underlying event contributions near mid-rapidity. These new parameter sets lead to large changes in forward particle production yields, since they typically adjust showering parameters and multiple-interaction parameters.  The study below uses PYTHIA 6.222 given its ability to predict $\sqrt{s}$ = 200 GeV particle yields.  It remains an assumption that the agreement at $\sqrt{s}$ = 200 GeV will result in good predictive power for p+p collisions at $\sqrt{s}$ = 500 GeV.

23

The fast simulator treats the response of the EMcal to photons, electrons and positrons using parameters that give a good description of the data. The energy resolution of the EMcal is simulated as $\sigma_E/E \sim 0.15/\sqrt{E}$ where $\sigma_E$ represents the Gaussian width of the energy response distribution from the EMcal irradiated with monoenergetic photons, electrons or positrons of energy $E$. For each event the incident energy is blurred by $\delta E$, chosen from a Gaussian distribution having $\sigma_E = 0.15\sqrt{E}$. A cluster is attributed with transverse position resolution at the EMcal given by $\sigma_{x(y)} = 0.1 d_{cell}$, where the calorimeter is assumed constructed from regular cells having square transverse dimensions of side length $d_{cell}$. The simulations were done using $d_{cell} = 3.8$ cm, representing transverse dimensions of lead-glass blocks manufactured by IHEP, Protvino.

For charged hadrons, the fast simulator establishes the fraction of the incident hadron energy that appears in the EMcal from distributions simulated by GEANT. Although the reliability of hadron shower simulators is frequently questioned, the fraction of the hadron energy ($f = \Delta E_{EMcal} / E_{hadron}$) deposited in the electromagnetic calorimeter as predicted by GEANT is found to be consistent with distributions measured by the CDF collaboration for 57-GeV pion test beams [41]. Section IV gives further details of the full GEANT simulations. For the simulations below, an energy- and hadron-type independent dN/d$f$ distribution is used. The dN/d$f$ distribution is approximated by a linear decrease in probability as $f$ increases. The parameters for the fast simulation are an interaction probability ($P_{int} = 0.5$) and the maximum fractional energy deposited by the incident hadron in the EMcal ($f_{max} = 0.9$). The cluster from the hadron fast simulator is suppressed if a uniformly distributed random number is smaller than $P_{supr} = 0.95$. The suppression factor is obtained from the combined action of the preshower detector (a pair of plastic scintillator detector planes sandwiching a 2 radiation length lead converter) and the Hcal. The suppression factor is expected to increase with increasing hadron energy and for decreasing $f$. The $P_{supr} = 0.95$ value is estimated from full GEANT simulations for $E = 10$ GeV charged pions and $f > 0.7$.

Photon conversions were found to be a limiting background in the last low-mass DY experiment. That experiment [40] detected low-mass ($M > 4.5$ GeV/c$^2$) $e^+e^-$ dileptons from p+p collisions at the ISR at $\sqrt{s} = 53$ and 63 GeV. Photon conversions are explicitly simulated in the fast simulation model given the computed path length through materials of known radiation length. Simulation of conversions in the beam-pipe crossing and the first scintillator layer of the preshower detector are made. Photon conversions are identified as an electron or positron cluster following the fast simulation, if the conversion point in the preshower is beyond its half thickness; i.e., the energy loss from the pair created in photon conversion matches the energy loss of a single electron traversing the full thickness of the scintillator. A small inefficiency (3% for 0.5 cm thick scintillator) is attributed to suppression of photon conversions in the beam pipe.

Clusters from different particles are merged if the impact point at the calorimeter from a particle is found to be within a distance of $0.8 d_{cell}$ from another particle.

A key step in reduction of the photon conversion background is to establish if pairs of simulated clusters are found with reconstructed invariant mass between 0.02 and 0.2 GeV/c$^2$, consistent with expectations for $\pi^0 \rightarrow \gamma\gamma$ decay. Neutral pion decay represents the primary source of photons that can convert. Cluster pairs with this invariant mass are excluded from consideration of large-

mass pairs. Large mass pairs are formed from events with one or more clusters remaining in each of the two modules straddling the beam pipe. The estimated background is shown in Fig. VII-1. DY events are found to dominate over the estimated background.
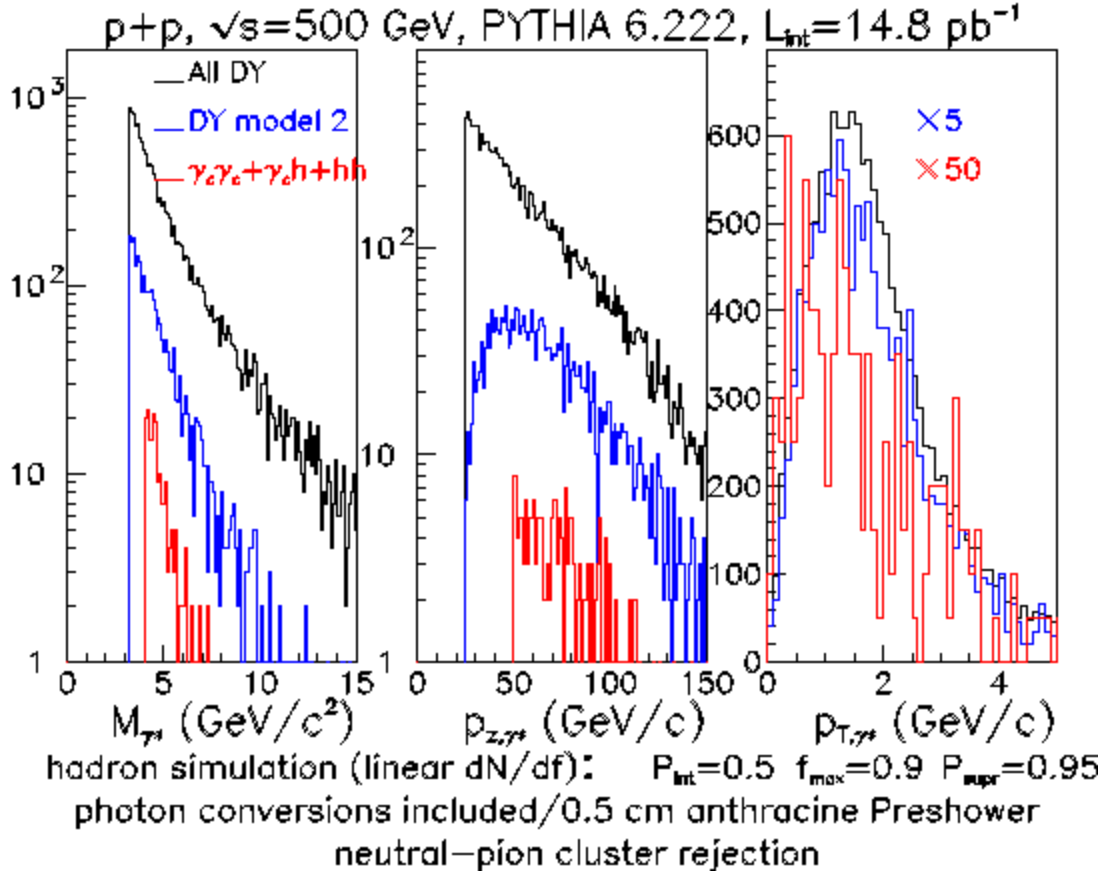


**Fig. VII-1** Estimate of backgrounds from photon conversions and hadrons, in comparison to the geometrical acceptance for $e^+e^-$ dileptons produced by the DY process. These simulations are for no magnetic field, corresponding to the run 12 setup as discussed in section IX.

Backgrounds from open heavy flavor production have been considered, and are expected to be small at large rapidity, unlike the case at smaller rapidities. For p+p collisions at $\sqrt{s}$=200 GeV, the dimuon mass distribution for the acceptance of the PHENIX muon arm was decomposed into contributing processes [32]. That decomposition found small contributions from open charm production for M > 4 GeV/c$^2$. Open beauty contributions were found to be ~2× larger than DY production near 4 GeV/c$^2$. Fig. VII-2 shows estimates for open beauty contributions to dilepton production for dileptons with $x_F$>0.1 at $\sqrt{s}$=500 GeV. Direct $gg \rightarrow b\bar{b}$ leading to both unlike-signed and like-signed dileptons is projected to be a 15% background, unlike the smaller rapidity case where the background is twice the DY signal. The reduced background is a result of detecting pairs at large $x_F$ where large $x$ gluons must be involved for the gluon fusion process. Furthermore, to create a background in the dilepton spectrum, both the $b$ jet and the $\bar{b}$ jet must be at large rapidity.
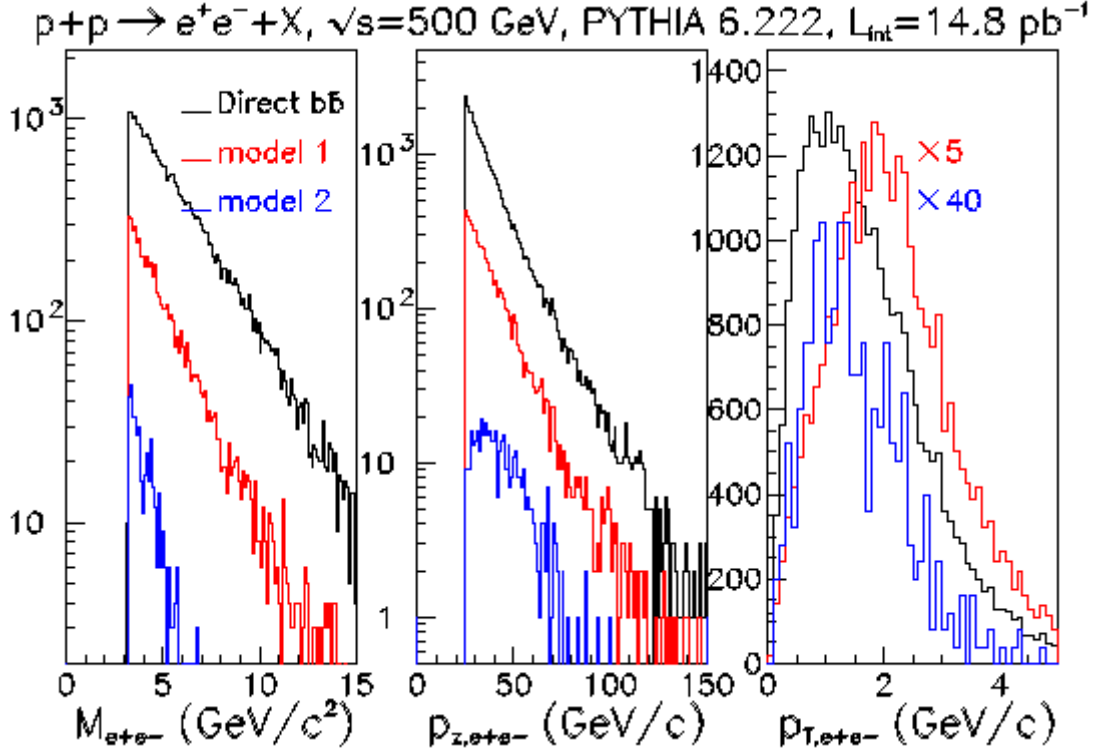
25

**Fig. VII-2** Estimate of backgrounds from direct open beauty production. This figure is to be compared to Fig. III-2 to get the ratio of Drell-Yan events to direct open beauty events. The black line is as predicted by PYTHIA 6.222, excluding detector acceptance. The red curves are for no magnetic field, at a possible future forward facility, as discussed in the text. The blue curves are for no magnetic field, corresponding to the run 12 $A_N$DY setup, as discussed in section IX. The open beauty background is twice larger than the Drell-Yan signal at the rapidity of the PHENIX muon arms [32]. The run 12 setup results in open beauty representing only a ~15% background to Drell-Yan production, since large-$x$ gluons must be involved to create a di-lepton pair with large $x_F$, and both jets must be at forward rapidity to make the di-lepton.

It is expected that 9400 DY events would be observed in model 2 apparatus with $M_{\gamma*} > 4$ GeV/c$^2$, $p_{z,\gamma*} > 25$ GeV/c ($x_F > 0.1$) and $p_{T,\gamma*} < 2$ GeV/c in a 150 pb$^{-1}$ data sample of transversely polarized proton collisions at $\sqrt{s}$=500 GeV with beam polarization of 50%. This would result in $\delta(A_N) \sim$ 0.018, with a small dilution from remaining background, whereas $|A_N| \sim 0.13$ is expected at large rapidity [11]. The $p_{T,\gamma*}$ cut is recommended by theory to ensure applicability of transverse-momentum dependent distribution (TMD) functions. Larger $p_{T,\gamma*}$ are expected from pQCD by the radiation of a hard gluon, therefore involving different physics than the "Sivers effect". Finally, the theoretical uncertainty on $|A_N|$ has been published [14] as a band of width $\Delta A_N$=0.05 near virtual photon $x_F \sim 0.3$. These calculations were done at $\sqrt{s}$=200 GeV, and with specific cuts on the virtual photon. A 150 pb$^{-1}$ data sample from an estimated delivered luminosity of 170 pb$^{-1}$ assumes that essentially all of the delivered integrated luminosity can be recorded. Prior experience with forward calorimetry has demonstrated that detector high voltages can be maintained at their operating point throughout the time used for setting up a RHIC store. In part, this is due to reduced backgrounds in the vicinity of the beam pipe due to the shielding from the ring magnet cryostats.

# VIII.  Choice and impact of interaction point

IP2 is the site of the former BRAHMS experiment. In RHIC Run 11 we staged both HCal modules, two 7x7 arrays of EMCal , and a 2-layer preshower detector with 3/16" Pb sheet between them, all facing the Blue beam ~4m downstream of the IP. Blue-beam and Yellow-beam Beam-Beam-Counters (BBCB and BBCY) and Zero-Degree Calorimeters (ZDCB and ZDCY) were installed and operated as trigger detectors and for beam monitoring. Each ZDC also had scintillator-strip position sensitive detectors used for local polarimetry.  A picture of the run-11 AnDY apparatus is shown in Fig. VIII-1.



**Fig. VIII-1**  Picture of the AnDY apparatus for RHIC run 11.  Not shown in the picture are the Yellow-beam facing beam-beam counter array and the zero-degree calorimeters.

IP2 is planned to  be the site for a test of coherent electron cooling (CeC) in the future.  The final CeC apparatus can not coexist with the apparatus required for AnDY.  AnDY measurements must be completed by RHIC run 13 so that IP2 can be used for CeC tests.  It is likely that partial staging of CeC apparatus may occur while AnDY is in IP2, based on discussions with physicists involved in the CeC project.  The CeC test fixes the timeline for the AnDY effort at IP2.

A systematic study of the impact of IP2 collisions on luminosity and operating conditions at IP6 and IP8 was conducted by Collider-Accelerator physicists during RHIC run 11.  The initial ring setup was adjusted in advance of the systematic study by the quench training of the IP2 DX magnets, as required for head-on (zero degree crossing angle) collisions of the beams at IP2.

This change necessitated changes in the procedure for removing the transverse separation of the beams to start collisions at IP2. The key step was to minimize the time that the beams were close to each other but were not in head on collision. Prior to implementing this step, tune shifts of the beams were signficiant resulting in large beam losses, primarily at the collimators but also a
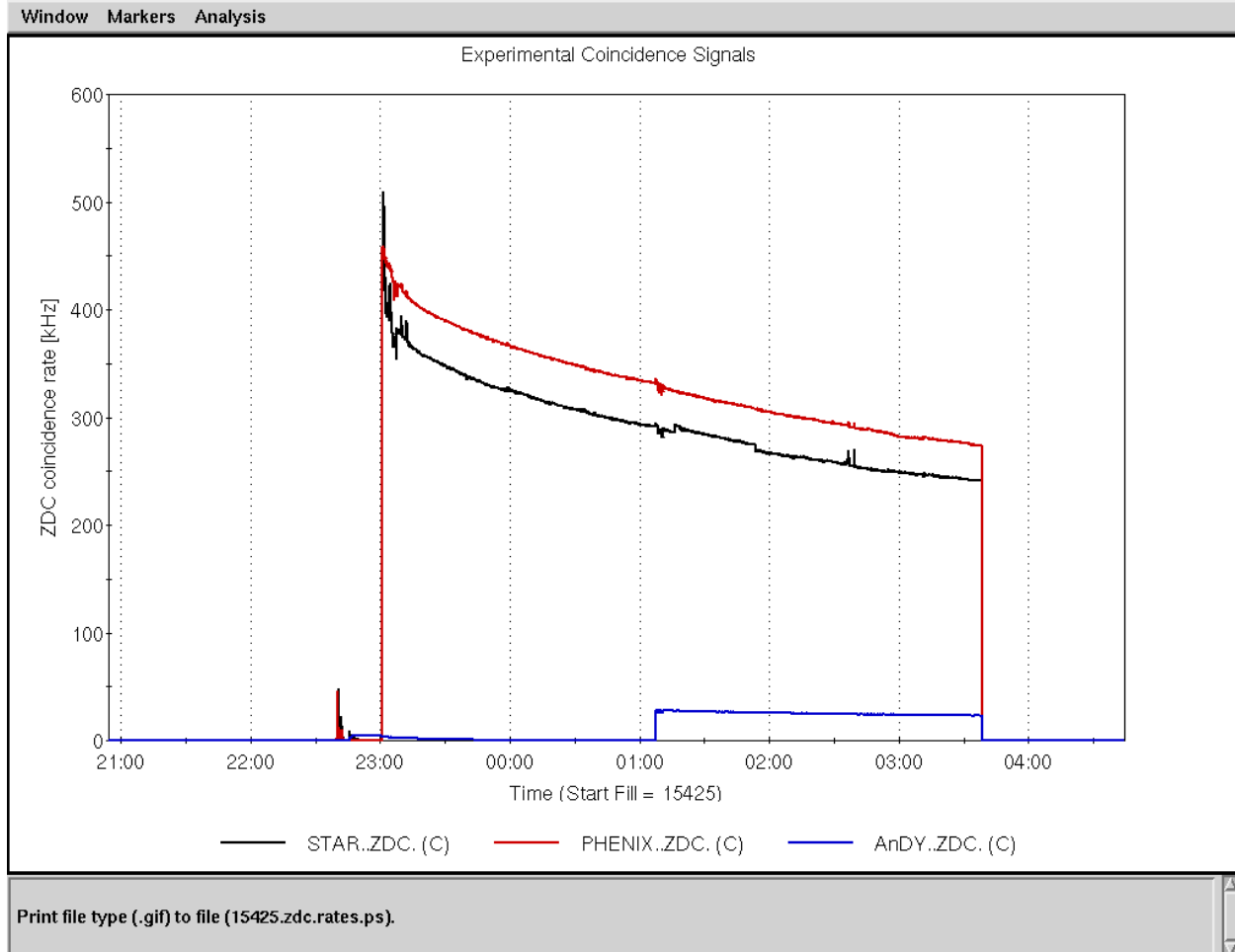


**Fig. VIII-2** ZDC coincidence rates at IP6 (black), IP8 (red) and IP2 (blue) versus time for RHIC fill 15425. The condition for initiating collisions at IP2 for this fill was that the average bunch intensity was $1.50 \times 10^{11}$ ions in each ring. IP2 collisions have minimal impact on luminosity at IP6 and IP8 in this fill. Similar results were observed for multiple fills. The sharp structures on top of the smooth reduction in ZDC coincidence rate are associated with CNI polarimeter measurements. The primary difference between the ZDC coincidence rates at IP2, IP6 and IP8 is associated with $\beta^*$ for the beams. The IP2 coincidence rate is smaller than expected, and likely reflects differences in threshold on the ZDC that await calibration by observation of the single-neutron peak in full-energy AuAu collisions.

source of backgrounds at IP6 and IP8. After optimization of the separation bump removal, a measurement plan was begun of initiating IP2 collisons when the beam intensity reached a threshold value. The starting point was average bunch intensity of $0.95 \times 10^{11}$. The threshold value was increased in average bunch intensity steps of $0.05 \times 10^{11}$ following evaluation of the impact in that store. In general, the impact on IP6 and IP8 was small for all thresholds. There were operational issues that could make the impact large. Specifically, when the threshold was at higher bunch intensities it was necessary to shift the tunes in the Yellow ring prior to the start of collisions at IP2 to compensate for beam-beam tune shift effects. The tune shifting was done

28

manually, and if it was done improperly then larger and longer lasting beam losses would result. The systematic increase in the start of IP2 collisions was followed until the threshold was increased to average bunch intensity of $1.55 \times 10^{11}$. There were two stores at this highest threshold. One store had minimal impact of IP2 collisions on IP6 and IP8, the other store had large impact due to issues with the tune shifting. At this point in the run, the focus was on integrating luminosity at IP6 and IP8, so the systematic threshold increases were terminated. Subsequently, IP2 collisions began at a fixed time after the declaration of physics running that coincided with the first CNI polarimeter measurement.

The conclusion from the systematic study is that IP2 collisions can be initiated without significant impact on operations at IP6 and IP8. The integrated luminosity requirements for a transverse spin Drell-Yan production measurement at IP2 can be met, with reduction of β* at IP2 and increased store length. Even larger integrated luminosities are possible if collisions at IP2 are initiated earlier in the store.

## IX. Staged implementation

The timeline in section X provides details of our staging of $A_N$DY. A schematic view of the apparatus envisioned for run-12 is shown in Fig. IX-1. The apparatus envisioned for run-13, including tracking stations and the magnet to measure charge sign, is shown in Fig. IX-2.



**Fig. IX-1** Schematic view of the present version of the detector elements intended for RHIC run 12. The components are (1) a multi-layer preshower scintillator array, sandwiching a 2 radiation length lead converter used for e/h discrimination; (2) a lead-glass electromagnetic calorimeter, consisting of 3.8 cm × 3.8cm × 45 cm lead glass bars from IHEP, Protvino and and 4.0cm x 4.0cm x 40cm PbGl bars from Yarevan borrowed from the JLAB BigCal collaboration;(3) an existing hadron calorimeter built for AGS-E864 [36]; and (4) a realistic beam pipe, consisting of beryllium, aluminum and stainless steel sections. Not shown are beam-beam counters and zero-degree calorimeters

30

**Fig. IX-2** Schematic view of the present version of the GEANT model, used for establishing detector responses for background and signal estimates. This is a schematic of the apparatus intended for RHIC run 13. The model consists of (1) the magnetic field for the split-dipole magnet designed and used by the PHOBOS collaboration at IP2; (2) a multi-layer preshower scintillator array, sandwiching a 2 radiation length lead converter used for e/h discrimination; (3) a lead-glass electromagnetic calorimeter, consisting only of 3.8 cm × 3.8cm × 45 cm lead glass bars;(4) an existing hadron calorimeter built for AGS-E864 [36]; (5) tracking stations for charge sign discrimination (fiber planes discussed in the text are not yet included) and (6) a realistic beam pipe, consisting of beryllium, aluminum and stainless steel sections. Not shown are beam-beam counters and zero-degree calorimeters
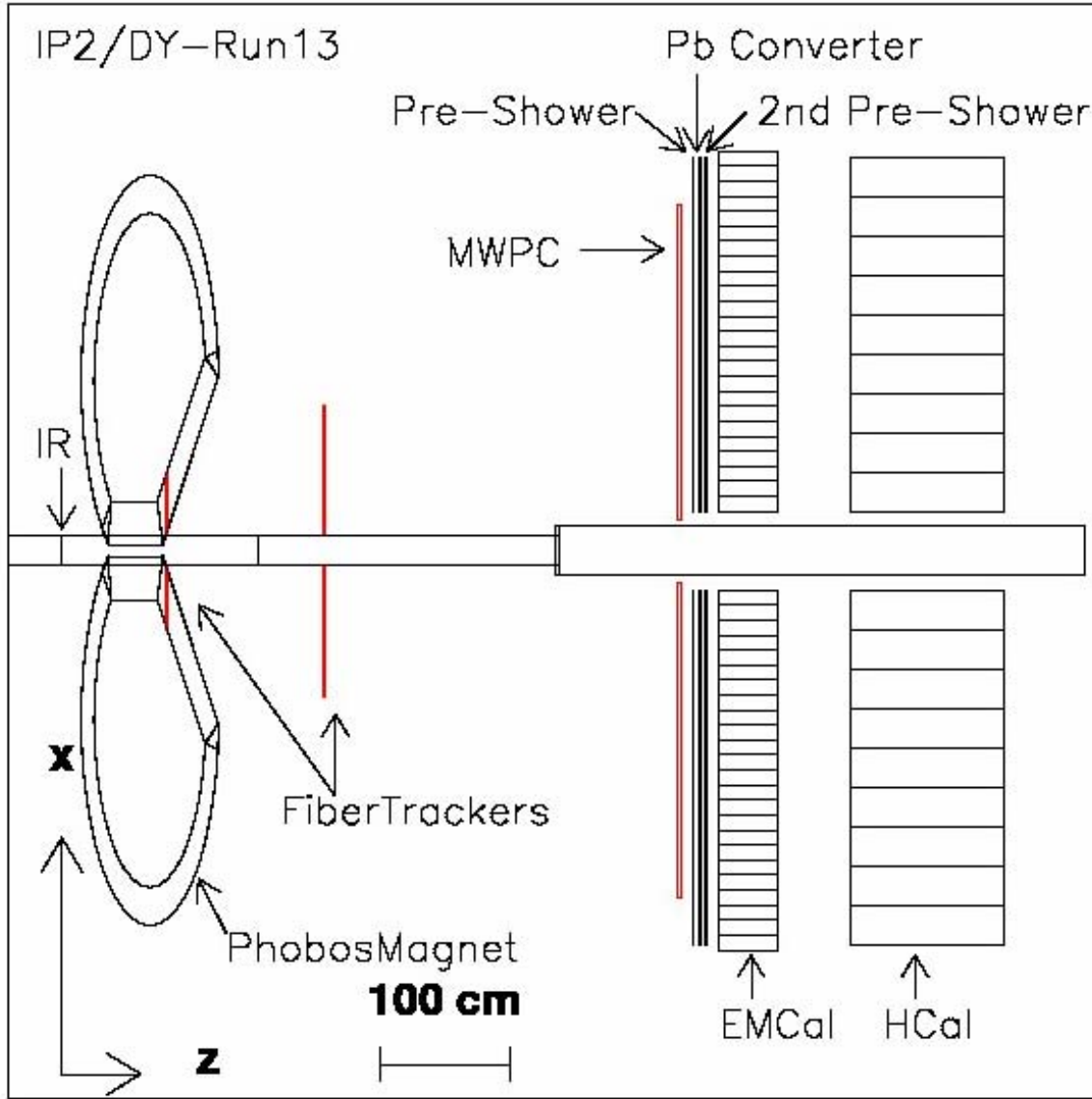
# X. Timeline, costs and manpower

In run12, we intend to see whether we can measure Drell-Yan signals using just the EMcal and Hcal without using charge-sign discrimination. In run13, we will investigate the additional background suppression provided by tracking through a magnetic field to improve signal to background and to lower the $M^2$ at which we can detect DY virtual photons. The details of our plan are available in a resource-loaded schedule whose output is shown in summary form below.
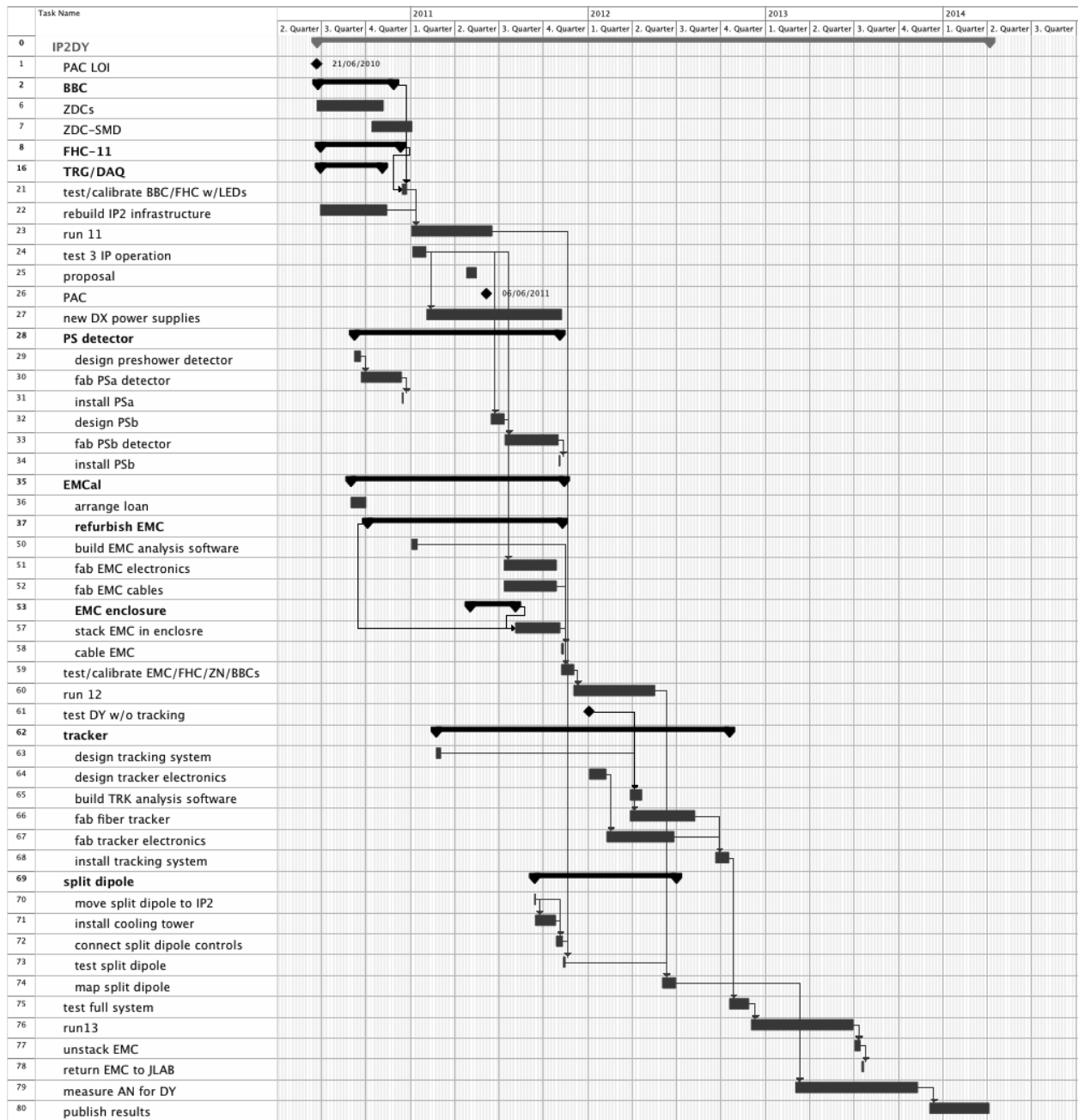
We use an existing data acquisition system at IP2 that we used for tests in run11. The data acquisition system is connected to the HPSS (High Performance Storage System) mass storage system in the RCF (RHIC Computing Facility) via single mode fibers previously used by the BRAHMS experiment. The data collected is archived into HPSS onto LTO3 media.

We will begin installation of our borrowed electromagnetic calorimeter (EMcal) as soon as we receive approval from the PAC. Each cell of BigCal will be tested for transmissivity at IP2 prior to installation. In our test of the 120 cells we used in Run11, we found that ~10% of these had measurable radiation damage. These were annealed using a small UV lamp setup that took ~24 hours to clear the discoloration and restore transmission to the level of the "un-radiation-damaged" cells. PMTs and bases will be refurbished as needed at this point in the testing as well. We believe that the time scale for determining the requirements for a low-x DY program at RHIC make it essential to complete our test program befor run14.

A charge/neutral (Z/N) detector is essential to our test of DY reconstruction based on EM calorimetry alone in run12. We believe from our simulations and run 11 tests that hadronic background can be significantly reduced by using a simple pre-shower detector in front of an EMcal. The Z/N detector is expected to consist of a 2 $L_{rad}$ thick layer of Pb sandwiched between layers of scintillator slats.

We will begin serious planning for charge-sign measurements at IP2 for run13 as soon as we are approved. If our EMcal based tests in run12 convince us that charge-sign is not necessary for reconstruction of low-mass (M>4 GeV) virtual photons, we may choose not to construct tracking chambers, but that will depend on data, not simulations. Our simulations have already convinced us that tracking stations in the split-dipole, just downstream of the magnet, and, ideally although not essentially, directly in front of the EMcal will give us sufficient information on electron charge to provide charge-sign measurements if needed. The 3$^{rd}$ tracking station, the one in front of the Emcal, will supplement the position resolution we obtain from cluster analysis in the EMCal. We will be designing fiber-based tracking planes for use near the magnets and to cover the 2 m$^2$ surface of the EMcal system so that we can fabricate these detectors for installation following run12.

We currently plan to install the tracking system at IP2 for run13. We note that a position sensitive detector in front of the EMCal is essential to using it for 500 GeV $\pi^0$ reconstruction at high $x_F$, so this is a detector system that will have a life as a shower-max detector well beyond AnDY. Once we have completed $A_N$DY we intend to make our results known quickly so that they can be factored into detector upgrade plans for other RHIC detectors.

Gantt chart — project schedule (2011–2014, by quarter)

| ID | Task Name | Notes |
|---|---|---|
| 0 | IP2DY | |
| 1 | PAC LOI | 21/06/2010 |
| 2 | **BBC** | |
| 6 | ZDCs | |
| 7 | ZDC-SMD | |
| 8 | **FHC-11** | |
| 16 | **TRG/DAQ** | |
| 21 | test/calibrate BBC/FHC w/LEDs | |
| 22 | rebuild IP2 infrastructure | |
| 23 | run 11 | |
| 24 | test 3 IP operation | |
| 25 | proposal | |
| 26 | PAC | 06/06/2011 |
| 27 | new DX power supplies | |
| 28 | **PS detector** | |
| 29 | design preshower detector | |
| 30 | fab PSa detector | |
| 31 | install PSa | |
| 32 | design PSb | |
| 33 | fab PSb detector | |
| 34 | install PSb | |
| 35 | **EMCal** | |
| 36 | arrange loan | |
| 37 | **refurbish EMC** | |
| 50 | build EMC analysis software | |
| 51 | fab EMC electronics | |
| 52 | fab EMC cables | |
| 53 | **EMC enclosure** | |
| 57 | stack EMC in enclosre | |
| 58 | cable EMC | |
| 59 | test/calibrate EMC/FHC/ZN/BBCs | |
| 60 | run 12 | |
| 61 | test DY w/o tracking | |
| 62 | **tracker** | |
| 63 | design tracking system | |
| 64 | design tracker electronics | |
| 65 | build TRK analysis software | |
| 66 | fab fiber tracker | |
| 67 | fab tracker electronics | |
| 68 | install tracking system | |
| 69 | **split dipole** | |
| 70 | move split dipole to IP2 | |
| 71 | install cooling tower | |
| 72 | connect split dipole controls | |
| 73 | test split dipole | |
| 74 | map split dipole | |
| 75 | test full system | |
| 76 | run13 | |
| 77 | unstack EMC | |
| 78 | return EMC to JLAB | |
| 79 | measure AN for DY | |
| 80 | publish results | |

## References

[1] G. Altarelli, R.K. Ellis, M. Greco and G. Martinelli, Nucl. Phys. **B246** (1984) 12;
J.C. Collins, D.E. Soper and G. Sterman, Nucl. Phys. **B250** (1985) 199;
X. Ji, J.P. Ma and F. Yuan, Phys. Lett. **B597** (2004) 299.

[2] J. Adams *et al*. (STAR), Phys. Rev. Lett. **92** (2004) 171801;
B.I. Abelev *et al*. (STAR), Phys. Rev. Lett. **101** (2008) 222001.

[3] I. Arsene *et al*. (BRAHMS), Phys. Rev. Lett. **101** (2008) 042001.

[4] A. Airapetian *et al*. (HERMES), Phys. Rev. Lett. **103** (2009) 152002.

[5] R.A. Seidl et al. (Belle), Phys. Rev. Lett. 96 (2006) 232002.

[6] J. Collins, Nucl. Phys. B **396** (1993) 161.

[7] D. Sivers, Phys. Rev. D **41** (1990) 83; **43** (1991) 261.

[8] S.J. Brodsky, D.S. Hwang and I. Schmidt, Phys. Lett. B530 (2002) 99.

[9] J.C. Collins, Phys. Lett. **B536** (2002) 43.

[10] Z.-B. Kang, J.-W. Qiu, W. Vogelsang, F. Yuan, Phys. Rev. D83 (2011) 094001
[arXiv:1103.11591]; D. Boer [arXiv:1105.2543] (2011).

[11] M. Boglione, U. D'Alesio, F. Murgia, Phys. Rev. D **77** (2008) 051502.

[12] M. Anselmino , *et al.*, Phys. Rev. D **72** (2005) 094007.

[13] D. Boer, P.J. Mulders, P. Pijlman, Nucl. Phys. B **667** (2003) 201.; X. Ji, J. Qiu, W.
Vogelsang, F. Yuan, Phys. Rev. Lett. **97** (2006) 082002.

[14] A. Adare *et al.* (PHENIX), Phys. Rev. Lett. **103** (2009) 012003.

[15] B.I. Abelev *et al.* (STAR), Phys. Rev. Lett. **101** (2008) 222001.

[16] D. de Florian, R. Sassot, M. Stratmann, W. Vogelsang, Phys. Rev. D **80** (2009) 034030.

[17] S.S. Adler *et al.* (PHENIX), Phys. Rev. Lett. **95** (2005) 202001.

[18] J. Adams *et al.* (STAR), Phys. Rev. Lett. **97** (2006) 152302.

[19] E. Braidot (for STAR), *Proceedings of the 45$^{th}$ Rencontres de Moriond*, La Thuile (2010)
[arXiv:1005.2378].

[20]  G.L. Kane, J. Pumplin, W. Repko, Phys. Rev. Lett. **41** (1978) 1689.

[21]  D. de Florian, R. Sassot, M. Stratmann, Phys. Rev. D **75** (2007) 114010.

[22] B.E. Bonner *et al.*, Phys. Rev. Lett. **61** (1988) 1918;
    A.Bravar  *et al.*, *ibid.* **77** (1996) 2626;
    D.L. Adams *et al.*, Phys. Lett. B **261** (1991) 201; **264** (1991) 462; Z. Phys. C **56** (1992) 181;
    K. Krueger *et al.*, Phys. Lett. B **459** (1999) 412;
    C.E. Allgower *et al.*, Phys. Rev. D **65** (2002) 092008;
    S. Saroff *et al.*, Phys. Rev. Lett. **64** (1990) 995;
    B.E.Bonner  *et al.*, Phys. Rev. D **41** (1990) 13;
    R.D. Klem *et al.*, Phys. Rev. Lett. **36** (1976) 929;
   W.H. Dragoset *et al.*, Phys. Rev. D **18** (1978) 3939.

[23]  C. Bourrely, J. Soffer, Eur. Phys. Journ. C **36** (2004) 371.

[24]  B. Lundberg *et al.*, Phys. Rev. D **40** (1989) 3557.

[25]  M. Burkardt, Nucl. Phys. **A735** (2004) 185.

[26]  J. Qiu, G. Sterman, Phys. Rev. D **59** (1998) 014004.

[27]  C. Kouvaris, J. Qiu, W. Vogelsang, F. Yuan, Phys. Rev. D **74** (2006) 114013.

[28]  D. Boer, W. Vogelsang, Phys. Rev. D **69** (2004) 094025.

[29]  B.I. Abelev *et al.* (STAR), Phys. Rev. Lett. **99** (2007) 142003.

[30]  A. Adare *et al.* (PHENIX), Phys. Rev. Lett. **98** (2007) 232002.

[31]  *Report to the Nuclear Science Advisory Committee by the Subcommittee on Performance Milestones*, 2008   [http://www.er.doe.gov/np/nsac/docs/PerfMeasEvalFinal.pdf]

[32]  *Transverse-Spin Drell-Yan Physics at RHIC*, L.C. Bland *et al.*
[http://spin.riken.bnl.gov/rsc/write-up/dy-final.pdf]

[33]  T.A. Armstrong *et al.* (E864), Nucl. Inst. Meth. A **406** (1998) 227.

[34]  C. Perkins (for the STAR collaboration), to appear in the *proceedings for Quark Matter 2009*, Knoxville [arXiv:0907.4396].

[35]  S.J. Brodsky, A.S. Goldhaber, B.Z. Kopeliovich, I. Schmidt, Nucl. Phys. B **807** (2009) 334.

[36]  B.B. Back *et al.* (PHOBOS), Nucl. Instr. Meth. A **499** (2003) 603.

[37]  M. Brennan, "*9MHz Acceleration System for Protons in RHIC*", RHIC spin collaboration meeting, 16 Dec 2008 [http://www.phenix.bnl.gov/WWW/publish/shura/RSC/2008/2008-12-16/9MHz_16dec2008.ppt]

[38]  L.C. Bland (for STAR), *Proceedings of the Xth Advanced Research Workshop on High Energy Spin Physics, Dubna* (2003) [hep-ex/0403012].

[39]  C. Kourkoumelis, *et al*  Phys. Lett. **91B** (1980) 475.

[40]  E. Gerchtein, M. Paulini, *Proceedings of Computing in High Energy and Nuclear Physics*, La Jolla (2003) [physics/0306031];
       P.A.M. Fernandez (for CDF), *Proceedings of the 12th International Conference on Calorimetry in High Energy Physics* (CALOR06), Chicago (IL), (2006) [hep-ex/0608081].